Eur. Phys. J. C 55, 553–575 (2008)
DOI 10.1140/epjc/s10052-008-0610-x

THE EUROPEAN PHYSICAL JOURNAL C

Regular Article – Theoretical Physics

Parton distributions for LO generators

A. Sherstnev[1,a,b], R.S. Thorne[2,c]

[1] Cavendish Laboratory, University of Cambridge, JJ Thomson Avenue, Cambridge, CB3 0HE, UK
[2] Department of Physics and Astronomy, University College London, WC1E 6BT, UK

Received: 21 November 2007 / Revised version: 31 March 2008 /
Published online: 16 May 2008 –

Abstract. We present a study of the results obtained by combining LO partonic matrix elements with either LO or NLO parton distributions. These are compared to the *best* prediction using NLO for both matrix elements and parton distributions. The aim is to determine which parton distributions are most appropriate to use in those cases where only LO matrix elements are available, e.g. as in many Monte Carlo generators. Both LO and NLO parton distributions have flaws, sometimes serious, for some processes, so a modified *optimal* LO set is suggested. We investigate a wide variety of processes, and the new modified LO* PDF works at least as well as, and often better than, both LO and NLO PDFs in nearly all cases.

1 Introduction

It has long been known that for certain regions of x there can be big differences between parton distributions extracted at different orders of perturbative QCD (see for example [1] for a discussion). Moreover, these differences between LO, NLO, and NNLO partons are much more significant than those between parton distributions extracted by various groups. This happens due to important missing higher order corrections in the splitting functions that determine the parton evolution, and in the cross-sections governing their extraction by comparison to experimental data (mainly from structure functions in deep inelastic scattering). In particular, use of parton distributions of the wrong order can lead to incorrect conclusions on the size of the small-x gluon, shown in Fig. 1, and consequently on the importance of corrections due to shadowing, saturation etc. at small x.

This large change in the size of parton distributions as one changes the perturbative order means that the combination of the respective order of the parton distribution function (PDF) and the accompanying matrix element is an important issue when calculating the cross-section for any physical process [2]. Traditionally, LO PDFs are thought to be the best choice for use with LO matrix elements, such as those available in many LO Monte Carlo programs, though it has been recognised that all such results should be treated with care. However, recently an alternative viewpoint has appeared, and it has been suggested that NLO PDFs may be more appropriate [3]. The argument is that NLO cross-section corrections are often small, and the main change in the total cross-section in going from LO to NLO is due to the PDFs. Indeed, there has already been an investigation of the use of NLO PDFs for the underlying event [4] at the tevatron. There is a big difference in the results when using CTEQ6L and CTEQ6.1M PDFs [5] due to the changes in the gluon, though agreement can be reached by significant retuning. However,

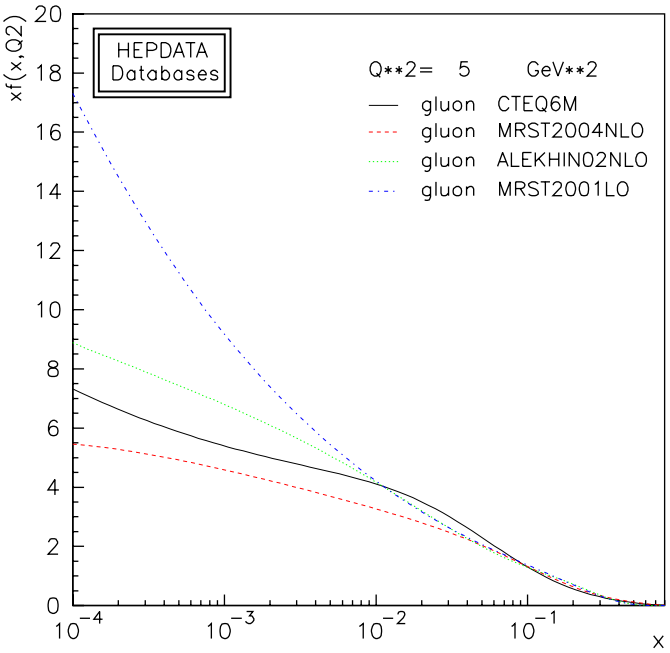

Fig. 1. A comparison of various gluon distributions at NLO and a gluon distribution at LO. There is significant variation in the NLO distributions, but the LO distribution is a qualitatively different shape from all of them

[a] Moscow State University, Moscow, Russia (on leave)
[b] e-mail: cherstn@hep.phy.cam.ac.uk
[c] Royal Society University Research Fellow

this retuning will potentially affect predictions for other quantities.

In this article we investigate the differences in predictions obtained for a variety of physical quantities combining different PDFs with LO matrix elements. In each case we assume NLO PDFs combined with NLO matrix elements represent the best prediction – the *truth*.[1] The different processes chosen rely on a variety of input parton distributions and on various ranges of x and Q^2 in order for us to try to make our conclusions as all-encompassing as possible. We interpret the features of the results noting that there are significant faults if one uses exclusively either LO or NLO PDFs. We hence attempt to minimise this problem, and investigate how a best set of PDFs for use with LO matrix elements may be obtained.

2 Parton distributions at different orders

Let us briefly explain the reasons for the origins of the differences between the parton distributions at different perturbative order. The qualitative difference between the LO and NLO gluon distribution is shown in Fig. 1. Clearly the LO gluon is much larger at small x than any NLO gluon at $Q^2 = 5\,\mathrm{GeV}^2$. The evolution of the gluon at LO and NLO is quite similar, so at larger Q^2 the relative difference is smaller, but it always remains significant. At $Q^2 = 1$–$2\,\mathrm{GeV}^2$ the difference is even more marked, with NLO gluon distributions becoming valence-like, or even negative at very small x, while the LO distribution remains large. This difference in the gluon distributions is a consequence of quark evolution, rather than gluon evolution. The small-x gluon is determined by $\mathrm{d}F_2/\mathrm{d}\ln Q^2$, which is directly related to the Q^2 evolution of the quark distributions. The quark–gluon splitting function P_{qg} is finite at small x at LO but develops a small-x divergence at NLO (and further $\ln(1/x)$ enhancements at higher orders), so the small-x gluon needs to be much bigger at LO in order to fit structure function evolution.

There are also significant differences between the LO and NLO quark distributions, as shown in the left of Fig. 2. Before analysing these in detail it is important to realise that beyond LO the parton distributions are factorisation scheme dependent. We conventionally take NLO to mean "NLO in the $\overline{\mathrm{MS}}$ factorisation scheme", and indeed this is the NLO distribution used in the left of Fig. 2. In order to illustrate the difference between orders we also show the comparison of the $\overline{\mathrm{MS}}$ scheme distribution at NLO and the DIS scheme distribution in the right of Fig. 2. In the DIS scheme the NLO coefficient functions relating parton distributions to structure functions are zero. Hence, if the LO parton distributions and NLO distributions produced identical structure functions, the right and left plots in Fig. 2 should be the same. Indeed, there are obvious similarities, both LO and NLO DIS scheme quark distributions being larger than NLO $\overline{\mathrm{MS}}$ scheme distributions at very high x and very low x. This is due to the effect of the NLO coefficient functions in the $\overline{\mathrm{MS}}$ scheme. Most particularly the quark coefficient functions for the structure functions in the $\overline{\mathrm{MS}}$ scheme have $\ln(1-x)$ enhancements at higher perturbative order, and the high-x quarks are smaller as the order increases. However, the LO quark distribution is depleted compared to the NLO DIS scheme quark distribution for $0.001 \leq x \leq 0.1$. And indeed, the LO fit to the structure function data is poor in this region.

Hence, while LO parton distributions are more similar to NLO DIS scheme distributions than NLO $\overline{\mathrm{MS}}$ scheme distributions (the gluons in DIS scheme and $\overline{\mathrm{MS}}$ scheme are similar except at very high x), there are some qualitative differences between LO and NLO in general. The LO gluon is much bigger at small x, and compared to $\overline{\mathrm{MS}}$ scheme the LO valence quarks are much bigger at high x. This is then accompanied by a significant depletion of the quark distribution for x in the region of 0.01, despite the fact that this leads to a poor fit to the data.

Let us examine the consequence of these differences when calculating physical cross-sections. In Fig. 3 we illustrate the ratio of the cross-sections produced for Drell–Yan production of a boson with invariant mass 80 GeV at tevatron energies using NLO $\overline{\mathrm{MS}}$ scheme parton distributions and NLO $\overline{\mathrm{MS}}$ scheme matrix elements (taken as the reference) [6], NLO $\overline{\mathrm{MS}}$ scheme parton distributions and LO matrix elements and LO parton distributions and LO matrix elements.[2] In this case for central rapidity, $y = 0$, both partons have $x = 0.04$, and the larger and smaller x, x_1 and x_2 are $0.04\exp(y)$ and $0.04\exp(-y)$ respectively. In this case it is the quark distributions that are probed.

Clearly we are generally nearer to the *truth* with the LO matrix element and NLO parton distribution [7] than with the LO matrix element and LO parton distributions [8]. However, this is always too small, since the NLO correction to the matrix element is positive. It is relatively y-independent, but there is the beginning of extra suppression at the highest y for the PDF[NLO]–ME[LO] calculation due to an additional enhancement in the NLO matrix element at high y, similar to the $\ln(1-x)$ enhancement for structure function coefficient functions. The depletion of the LO quark distributions for $x \sim 0.04$ leads to the extra suppression in the PDF[LO]–ME[LO] calculation. However, when probing the high-x quarks, the increase in the LO parton compensates for the increase in the NLO matrix element, and for $y > 2$ this gives the more accurate result. However, overall the shape as a function of y is much worse using the LO parton distributions than the NLO distributions.

We consider the same comparison, but for boson production at the LHC rather than the tevatron, in Fig. 4. In this case the central rapidity corresponds to $x = 0.006$, and we have to go to a higher rapidity than at the tevatron to be sensitive to large-x effects, but we have much more

[1] Of course, the full NNLO calculation is known for some processes, but we will avoid this further complication in this article.

[2] Since NLO matrix elements are most readily available in the $\overline{\mathrm{MS}}$ scheme, we will take this as the default, and henceforth NLO is intended to mean NLO in $\overline{\mathrm{MS}}$ scheme unless explicitly stated otherwise.

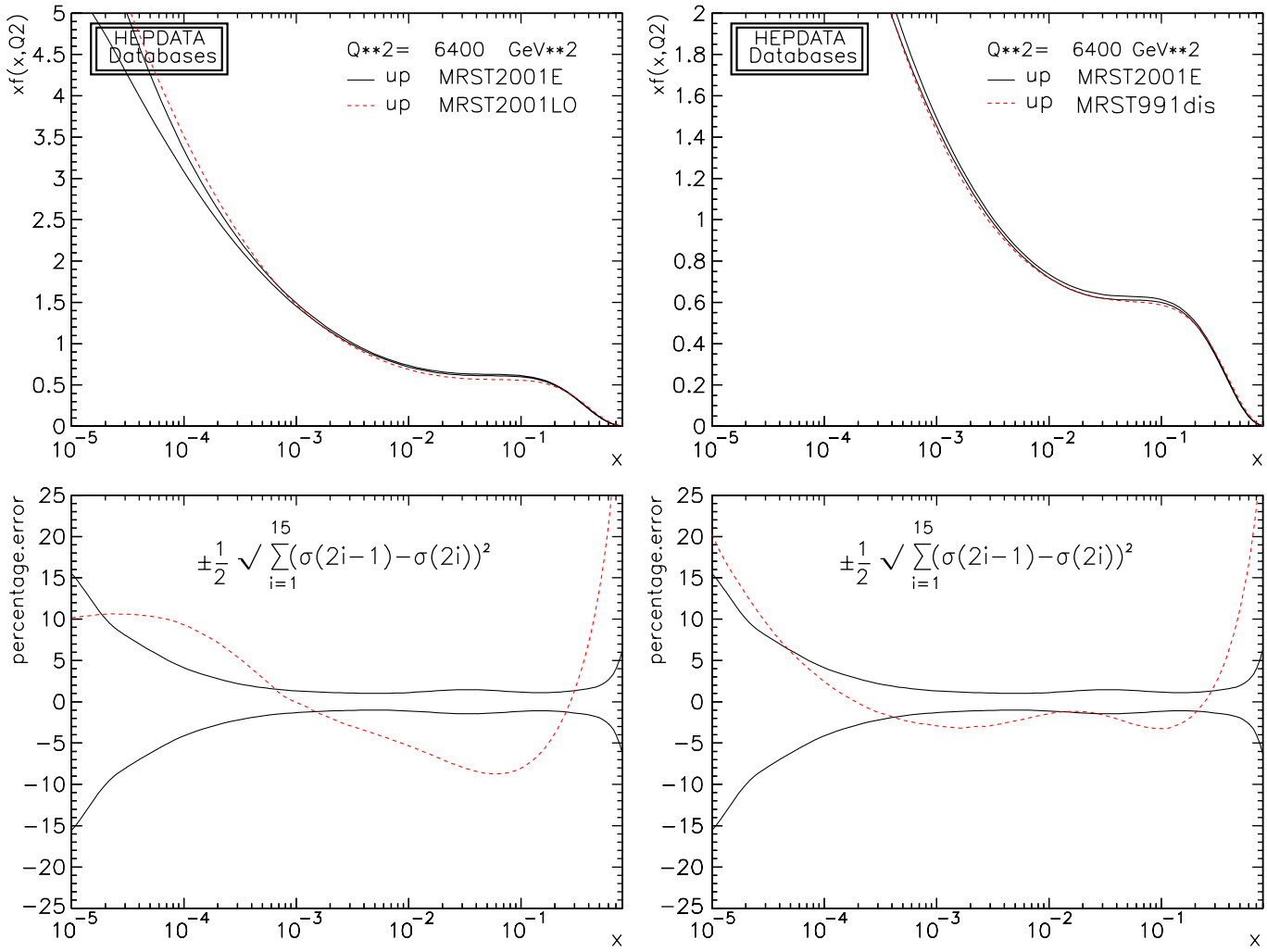

Fig. 2. The comparison of the up quark parton distribution at LO with that at NLO in the $\overline{\rm MS}$ factorization scheme (*left*) and the comparison between the NLO $\overline{\rm MS}$-scheme and DIS-scheme up quark distribution (*right*), both at at $Q^2 = 6400\,{\rm GeV}^2$. The *upper plots* show the uncertainty bands of the NLO $\overline{\rm MS}$ distribution and the *lower plots* the percentage uncertainty. In both cases this is compared to the central LO or DIS scheme distribution

sensitivity to small x. Again the PDF[NLO]–ME[LO] calculation is suppressed compared to the *truth*, but this time there is less change in shape at high rapidity, since even at $y = 3$ ($x_1 = 0.11$ and $x_2 = 0.0003$) we are barely reaching the regime of enhanced NLO partonic cross-sections. As for the tevatron, the PDF[LO]–ME[LO] result is even more suppressed, due to the depletion of quarks, though this begins to reduce at the highest y, mainly due to increases in small-x quarks at LO. The general conclusion is the same as for the tevatron – the NLO PDFs provide a better normalisation and a better shape.

This single quantity suggests that the opinion in [3] is correct, i.e. that NLO PDFs are more appropriate if one only has LO matrix elements. However, this is a very processes dependent statement. In order to demonstrate this we consider a quantity sensitive to the small-x gluon distribution, where the difference between the LO and NLO gluon distribution is due to missing higher order perturbative corrections. Let us consider the production of charm in DIS, i.e. $F_2^{c\bar{c}}(x, Q^2)$, where we take all charm as produced in the final state, i.e. we work in the fixed-flavour number scheme (FFNS). In this case the NLO coefficient function, $C_{2,g}^{c\bar{c},(2)}(x, Q^2, m_c^2)$, contains a divergence at small x not present at LO, in the same way that the quark–gluon splitting function does, the latter being responsible for the large difference between the LO and NLO gluon distributions at small x. In the left part of Fig. 5 we see the large effect of the NLO coefficient functions [9, 10]. When using NLO partons the LO matrix element result is well below the *truth* at low scales, and the shape is totally wrong. The structure function follows the shape of the gluon distribution at NLO, whereas the small-x divergence in the coefficient function provides a charm structure function that rises at small x in the same way that the NLO correction to P_{qg} provides a total $\mathrm{d}F_2/\mathrm{d}\ln(Q^2)$ that rises at small x. In the right part of Fig. 5 we see the result using the LO PDFs. In this case $F_2^{c\bar{c}}(x, Q^2)$ rises at small x even with the LO coefficient function, due to the rising gluon.

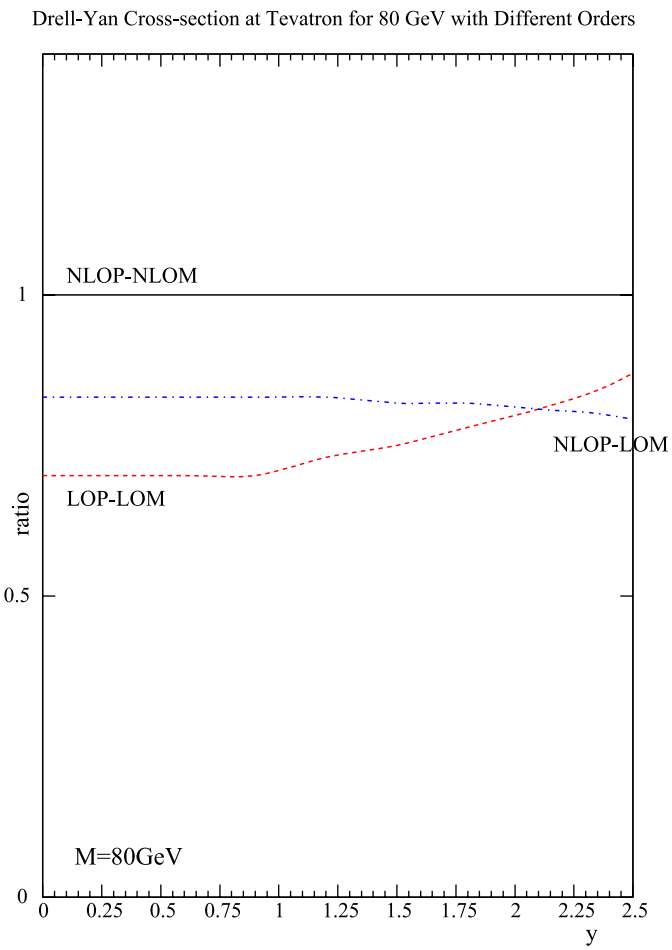

Fig. 3. Comparison of boson production at the tevatron using combinations of different orders of parton distributions and hard partonic cross-sections

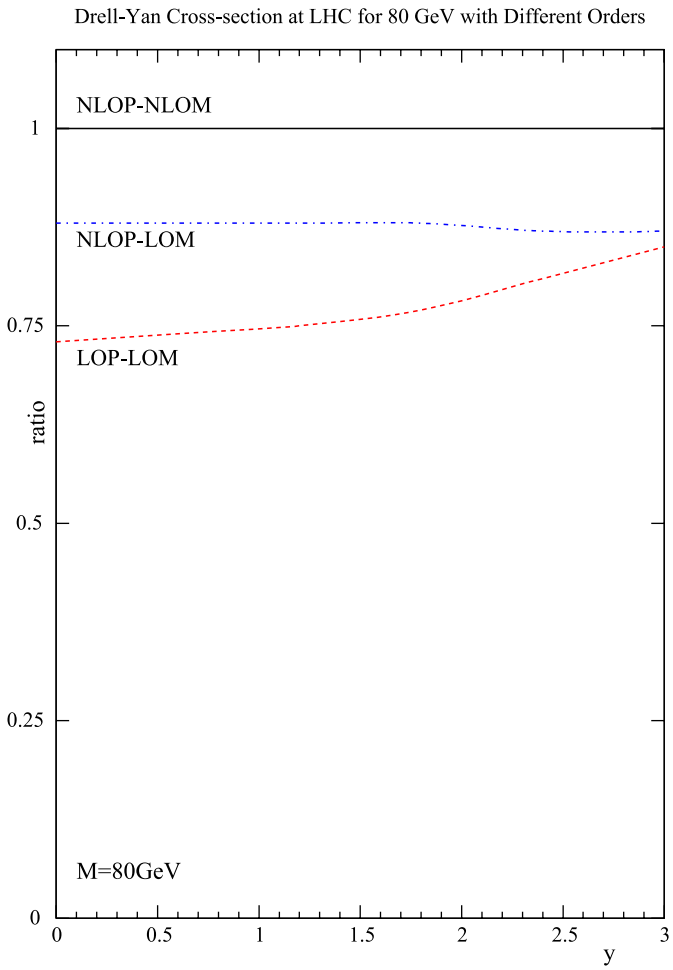

Fig. 4. The same as Fig. 3, but at LHC energies

Using the NLO coefficient function and the LO PDFs effectively double counts the small-x divergence, and the result is much too large and steep. All four results are shown together in Fig. 6. While the LO PDFs combined with LO coefficient functions is not a perfect match to the *truth* – after all the small-x divergences are not exactly the same in matrix element and splitting function – it is clearly far better than the other two approaches that either double count the small-x divergences, or include neither. In particular, in this case the NLO PDFs together with the LO matrix elements fail badly, providing a clear contradiction to the view in [3].

Hence, from these two simple examples alone we can draw the following conclusions. Sometimes it is better to use NLO PDFs if only LO matrix elements are known, and one can encounter significant problems with both normalisation and shape if LO PDFs are used. However, one can be completely wrong, particularly at small x, by using NLO partons with LO matrix elements, due to effective zero-counting of small-x divergences. One could finish here and conclude that it is necessary to consider on a case by case basis, and, in any analysis that uses LO Monte Carlo generators, sometimes use LO PDFs and sometimes NLO PDFs, depending on the particular process under consideration. However, we will continue our investigation rather than accepting this pessimistic conclusion and attempt to discover whether there are some *optimal* partons that have the desirable features of both LO and NLO PDFs.

3 Improved LO parton distributions

In order to make progress in finding some *optimal* set of PDFs for use with LO matrix elements we need to understand fully the differences between LO and NLO partons. As seen by comparison with the NLO DIS scheme partons in Fig. 2, part of the dip in LO quarks compared to NLO is due to an extra coefficient function contribution at NLO (particularly for $x \sim 0.1$), but it is mostly a problem at LO – the size and extent of the depletion from $x = 0.1$–0.001 is reflected in the fit quality. At LO, compared to NLO (and higher orders), missing terms in $\ln(1-x)$ and $\ln(1/x)$ in the coefficient functions and/or evolution lead to a gluon that is much bigger as $x \to 0$ and valence quarks that are much larger as $x \to 1$ in order to compensate. From the momentum sum rule there are then not enough partons to go

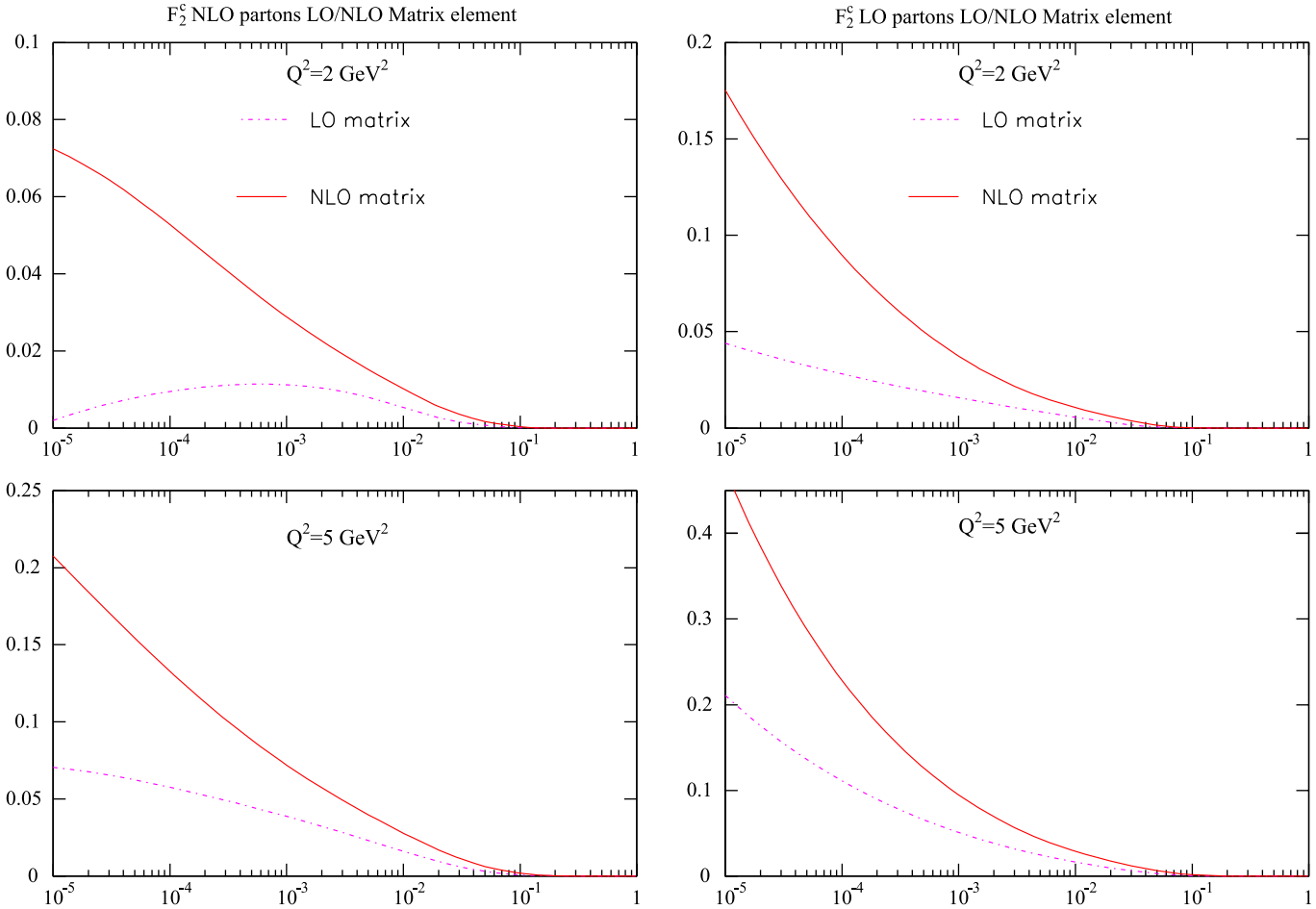

Fig. 5. A comparison of charm production at HERA using LO and NLO coefficient functions and NLO parton distributions (*left*), and using LO parton distribution functions (*right*)

around; hence the depletion in the quark distributions at moderate to small x.

This depletion leads to a bad global fit at LO, particularly for HERA structure function data that are very sensitive to quark distributions at $x \sim 0.01$. In practice the lack of partons at LO is partially compensated by a LO extraction of $\alpha_s(M_Z^2) \sim 0.130$, i.e. the very large coupling constant leads to quicker evolution, making up for the higher order corrections and/or smaller parton distributions in some regions. This results in one obvious modification. It is helpful to use the NLO definition of the coupling constant in a LO fit to parton distributions. Because of quicker running at NLO, LO and NLO couplings with the same value of $\alpha_s(M_Z^2)$ become very different at lower scales where DIS data exist, as shown in Fig. 7. Alternatively, near $Q^2 = 1\,\mathrm{GeV}^2$ the NLO coupling with $\alpha_s(M_Z^2) = 0.120$ is similar to the LO coupling with $\alpha_s(M_Z^2) = 0.130$. Consequently, the NLO coupling with $\alpha_s(M_Z^2) = 0.120$ is much bigger than the LO coupling with $\alpha_s(M_Z^2) = 0.120$, and will do a much better job in fitting the low-Q^2 structure function data. Hence, the use of the NLO coupling helps alleviate the discrepancy between the parton distributions at different orders. Indeed, the NLO coupling is already used in some CTEQ LO PDFs and in Monte Carlo generators.

However, even with this modification the LO fit is still poor compared with NLO, and the partons are still depleted in some regions. The problems caused due to the depletion of partons have led to a suggestion [11] that relaxing the momentum sum rule for the input parton distributions could make LO partons rather more like NLO partons where they are normally too small, while allowing the resulting partons still to be bigger than NLO where necessary, i.e. the small-x gluon and high-x quarks.

Relaxing the momentum sum rule at input[3] and using the NLO definition of the strong coupling does dramatically improve the quality of the LO global fit (though a K-factor of 1.3 is necessary for fixed target Drell–Yan data). We have $\chi^2 = 3066/2235$ for the standard LO fit, and this becomes $\chi^2 = 2691/2235$ for the modified fit. The data set fit is much the same as in [7] and the heavy flavour prescription used is that in [12], which is a little different from that for previous fits at LO. There is a particularly big improvement in the quality of the fit to HERA data. When using the NLO definition of the coupling we obtain $\alpha_s(M_Z^2) = 0.121$, which is a much more sensible

[3] The evolution automatically conserves momentum.

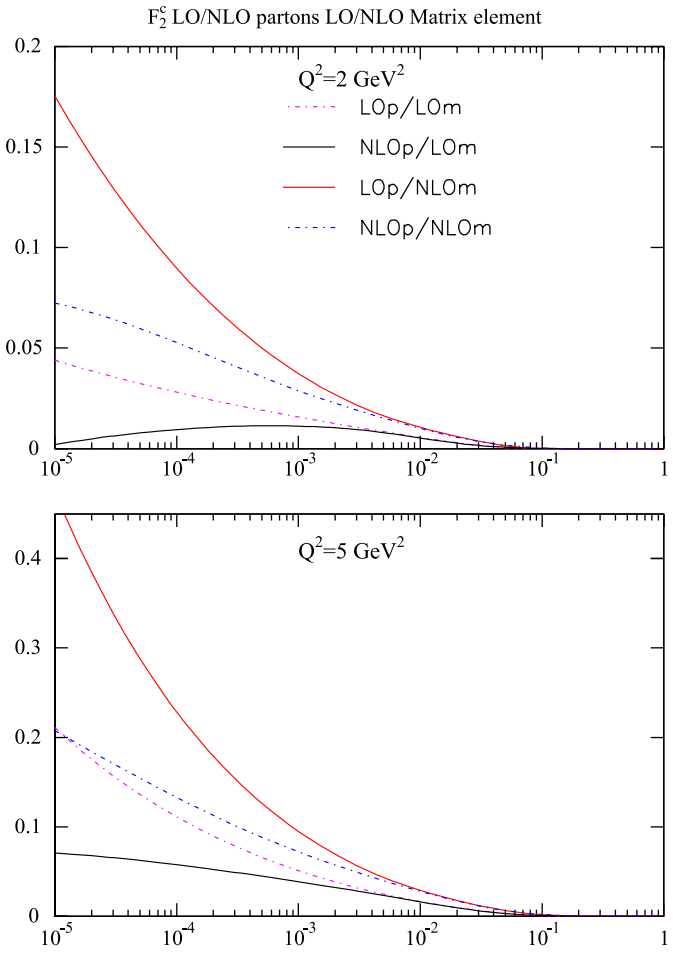

Fig. 6. A comparison of charm production at HERA using all combinations of LO and NLO partons and LO and NLO coefficient functions

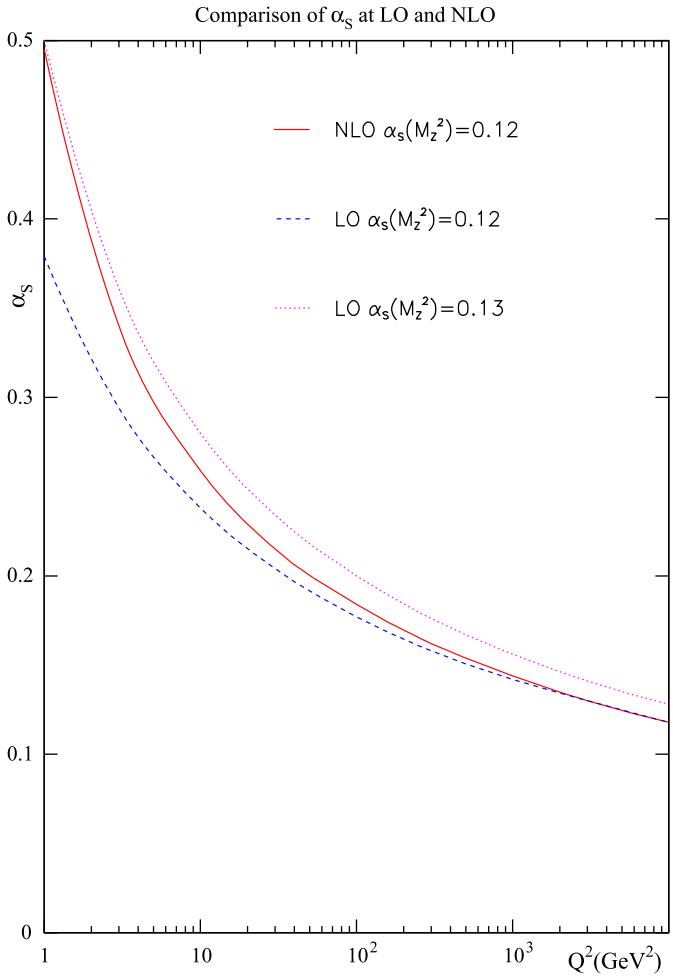

Fig. 7. Comparison of the LO and NLO definitions of α_s

result than in the pure LO fit. The momentum carried by input partons goes up to 113%. We denote the partons resulting from this fit as the LO* parton distribution functions.

The LO*, LO and NLO partons are compared in Fig. 8. One can see that the LO* quark distribution is bigger than at LO at $x < 0.1$, and only smaller than NLO for a small region centred slightly below $x = 0.1$. Similarly $g(x, Q^2)$ is significantly bigger at LO* than at LO, and much bigger than NLO at small x.[4] Hence, the LO* gluon distribution should do better than LO for gluon–gluon initiated processes (e.g. Higgs production), where K-factors are often much greater than unity.

We can make a simple test of the potential of these improved LO* partons by repeating the comparisons of the previous section. Consider Drell–Yan production at the LHC, shown in Fig. 9. Indeed, we are nearer to the *truth* with the LO matrix element and LO* PDFs than with either LO or NLO PDFs. Moreover, the shape using the LO* PDFs is of a quality similar to that using the NLO partons with the LO matrix element. So in this case LO* PDFs and NLO PDFs are comparably successful.

The exercise is also repeated for the charm structure function at HERA, as seen in Fig. 10. When using the LO coefficient function the LO* PDFs result is indeed nearest to the *truth* at low scales, being generally a slight improvement on the result using LO PDFs, and clearly much better than that using NLO PDFs. One would expect there to be a similar result for all processes dependent on the gluon distribution at small x, e.g. hadro-production of c and/or b quarks at the LHC.

These simple examples suggest that the LO* PDFs may well be a valuable tool for use with Monte Carlo generators at LO, combining much of the advantage of using the NLO distributions while avoiding the major pitfalls. However, the examples so far are rather unsophisticated. They are sufficient to show that something can go badly wrong in some cases, but in order to determine the best set of PDFs to use it is necessary to work a little harder. We need to examine a wide variety of contributing par-

[4] Both LO and LO* gluon distributions are smaller than NLO at very large x. This is because the increase in the LO quark distributions in this region allows for a good fit to the tevatron jet data without a significant high-x gluon distribution. The LO gluon distribution at very high x would be more similar to that at NLO in the DIS scheme [7].

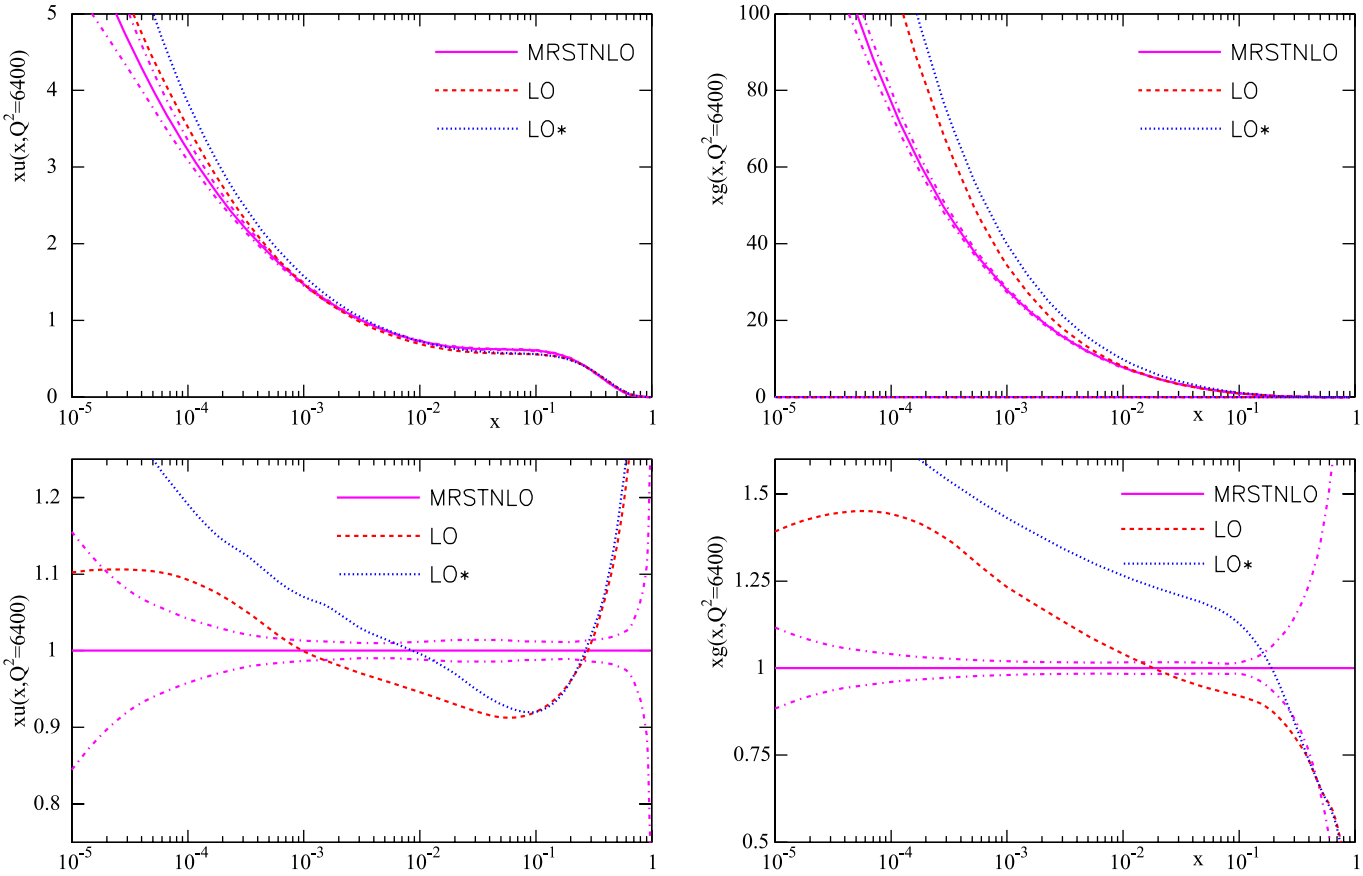

Fig. 8. Comparison between the LO, LO* and NLO up quarks (*left*) and between LO, LO* and NLO gluon (*right*)

ton distributions, both in type of distribution and range of x. Also, the above examples are both completely inclusive; they have not taken into account cuts on the data. Nor have they taken account of any of the possible effects of parton showering, which is, of course, one of the most important features of Monte Carlo generators. Hence, before drawing any firm conclusions we will make a wide variety of comparisons for different types of possible process at the LHC, using Monte Carlo generators to produce the details of the final state.

4 Details of different production mechanisms

We consider a variety of final states for proton–proton collisions at LHC energies. In each case we compare the cross-section with LO matrix elements and full parton showering for the three cases of LO, LO* and NLO parton distributions. We also include the results using a Monte Carlo generator with NLO matrix element corrections [13] together with NLO parton distributions, which we take to be the *truth*. If a process is not available in MC@NLO, we

Table 1. A list of investigated processes at the LHC, along with Monte Carlo codes and the hard QCD scales used in the calculations

Process	LO generator	NLO generator	QCD scale
$pp \to W \to \mu\nu$	CompHEP/HERWIG	MC@NLO	$\hat{s}$
$pp \to Wj \to \mu\nu j$	CompHEP/HERWIG	MCFM	$\hat{s}$
$pp \to Z/\gamma \to 2\mu$	CompHEP/HERWIG	MC@NLO	$\hat{s}$
$pp \to t, q$	CompHEP/HERWIG	MC@NLO	m_t
$g, g \to H$	CompHEP/HERWIG	MC@NLO	m_H
$pp \to Hqq$	CompHEP/HERWIG	VBFNLO	m_H
$pp \to b\bar{b}$	HERWIG	MC@NLO	$\sqrt{m_b^2 + \langle p_{\rm T}\rangle^2}$
$pp \to t\bar{t}$	CompHEP	MC@NLO	$\sqrt{m_t^2 + \langle p_{\rm T}\rangle^2}$
$pp \to jj$	CompHEP/HERWIG	JETRAD	$E_{\rm T}$

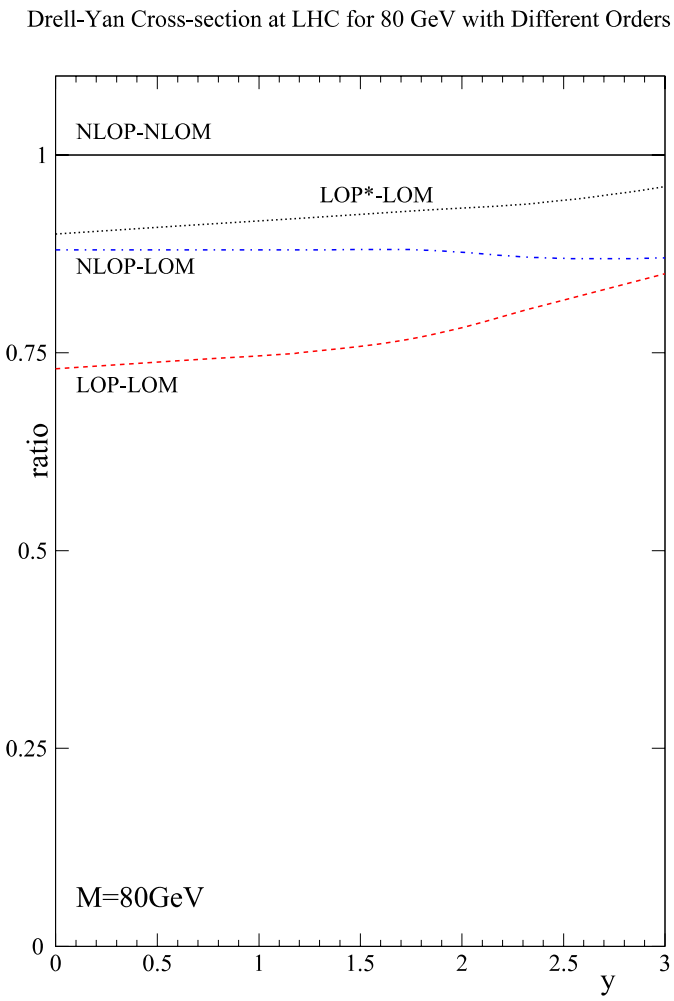

Fig. 9. Comparison of boson production at the LHC using combinations of different orders of parton distributions and hard partonic cross-sections, now including LO* PDFs

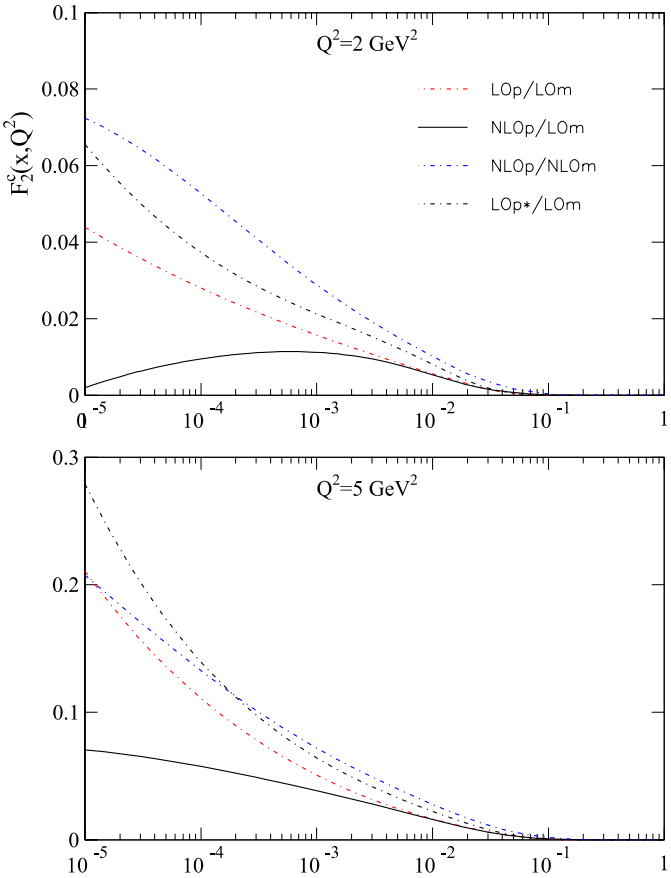

Fig. 10. A comparison of charm production at HERA using LO, NLO, and LO* parton distributions with LO coefficient functions and the *truth* of NLO PDFs with NLO coefficient functions

use the standard NLO approximation without the parton shower influence. The different examples span a range of values of x and hard scales and probe different combinations of parton distributions.

Table 1 reports generators [13–18] used and QCD scales applied in the calculations. As the main LO generator we use CompHEP interfaced with the FORTRAN package HERWIG, except $pp \to b\bar{b}$, where HERWIG is the more appropriate generator. The main NLO generator is MC@NLO except for the three processes $pp \to Hqq$, $pp \to Wj \to \mu\nu j$ and $pp \to jj$, which are not available in MC@NLO. The following parameters are used in the calculations: $m_W = 80.4\,\text{GeV}$, $m_Z = 91.176\,\text{GeV}$, $\Gamma_W = 2.028\,\text{GeV}$, $\Gamma_Z = 2.44\,\text{GeV}$, $\cos\theta_W = 0.2311$, $m_b = 4.85\,\text{GeV}$, $m_c = 1.65\,\text{GeV}$, $m_\mu = 105.66\,\text{MeV}$, $\alpha = 1/127.9$ (fixed), running α_s (according to the chosen PDFs).

4.1 W production at the LHC

We first revisit our previous LHC example of W production, but with full parton showering and an investigation of the total cross-section and p_T distribution as well as the pseudo-rapidity distribution. Hence, we consider the LO production mechanism of quark–antiquark annihilation where $x = 0.006$ at central pseudo-rapidity. The total cross-sections are shown in Table 2, and we see that all predictions using the LO matrix elements are lower than the *truth*, but that using the LO* PDFs is easily closest.

The distributions are seen in the upper part of Fig. 11, where the small plots are the ratio of the *truth* to each of our LO matrix element predictions. For the W-boson pseudo-rapidity distribution the LO partons give a result that is suppressed at central rapidities due to the depletion

Table 2. The total cross-sections $\sigma(pp \to W \to \mu\nu_\mu)$ at the LHC

Parton	Matrix element	σ (nb)	K-factor
NLO	NLO	21.1	
LO	LO	17.5	1.21
NLO	LO	18.6	1.13
LO*	LO	20.6	1.02

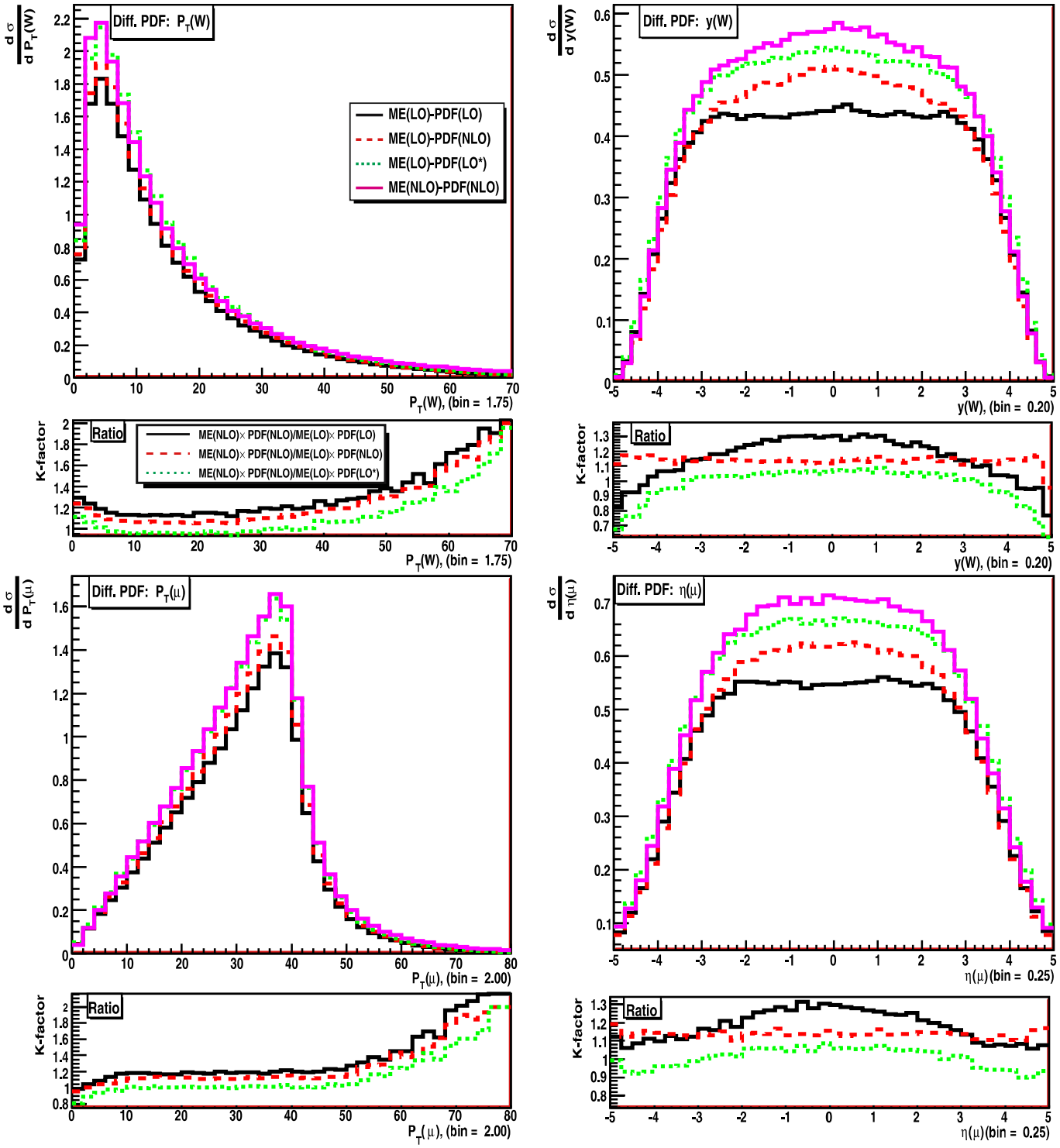

Fig. 11. The comparison between the competing predictions for the differential cross-section for W-boson production at the LHC (*left*) and for the resulting muon (*right*)

of quarks seen before. The LO* partons give a good representation of the *truth*, being just a little small at central rapidity and a bit large at the very highest rapidity. The NLO partons are slightly worse in normalisation, but overall are actually best in shape. They are a little low for very high rapidity, where the excess of LO* partons at very high and low x overcompensates for enhancement in the NLO matrix elements, while the NLO partons do not compensate at all. These high rapidities are outside the range of ATLAS and CMS but may be relevant at LHCb. The LO partons give too low a result at central rapidity due to the depletion for $x \sim 0.01$.

For the p_T distributions none of the PDFs gives a good representation of the shape with p_T. In particular, they all lead to predictions that are too small with increasing large p_T. At LO the p_T is simulated by a parton shower algorithm (in our case, by the HERWIG algorithm). By definition it underestimates the high-p_T region in comparison with the true NLO correction. As we will see, this type of effect is a recurring feature. It cannot be solved by defining PDFs and must be borne in mind whenever using LO Monte Carlo generators. Nevertheless, all PDFs produce rather similar shapes using the LO generator, but again the LO* PDFs give the best normalisation.

In the lower part of Fig. 11 we see the distributions for the final-state muon in the W decay. The conclusions are similar. Again for the rapidity distribution the LO* distributions are best in normalisation, and they indeed are an excellent approximation to the *truth*. The rapidity of the muon is usually a bit higher than that of the parent W so the effect right at the edge of the rapidity plot in the W case is not visible for the muon and would be smeared at even higher muon rapidity. The NLO partons are low in normalisation, but arguably best in shape. Again the LO PDFs fail worst at central rapidity. For the p_T distribution the NLO excess only sets in beyond ~ 50 GeV, but this is simply due to the intrinsic p_T of the muon from the W decay.

The range of x and "average" $\log \hat{x} = 0.5(\log_{10} x_1 + \log_{10} x_2)$ of the contributing partons are shown in Fig. 12. For the LO production mechanism $\hat{x}$ is centred on the line $x_1 x_2 = m_W^2/s$ with some width, whereas at NLO there is a slightly increased contribution from the region $x_1 x_2 > m_W/\sqrt{s}$, where one of the incoming partons emits a relatively hard parton before undergoing the annihilation, this hard parton providing some hard p_T to balance the W boson. A depletion is seen for the LO partons in the region $x = 0.001$–0.1.

Since the LHC initial state is dominated by gluons, processes with gluons in the initial state are of particular interest. In the W-production process both initial partons are quarks. Initial gluons appear in the associated production of W and one jet, and in this process we probe both quark and gluon PDFs. We calculated the total cross-section for all our previously considered cases, the LO matrix element with three PDFs and the *truth*. The NLO approximation was calculated by the MCFM program [19]. Reasonable cuts were applied in order to exclude kinematic regions where the LO matrix element has singularities. The total cross-sections are reported in Table 3. As we can see, the LO* PDFs give the best normalisation.

Table 3. The total cross-sections $\sigma(pp \to Wj \to \mu\nu_\mu j)$ at the LHC. Cuts: $p_T(j) > 20$ GeV, $|\eta(j)| < 5$

Parton	Matrix element	σ (nb)	K-factor
NLO	NLO	5.96	
LO	LO	4.66	1.28
NLO	LO	4.20	1.42
LO*	LO	5.43	1.10

4.2 Z/γ production at the LHC

Next we consider the rather similar process of quark–antiquark annihilation to Z/γ bosons, decaying to muons. In order to exclude the dangerous region $m_{\rm inv}(\mu\mu) \to 0$, where the matrix element at LO has a singularity, we apply some experimentally reasonable cuts $p_T > 10$ GeV and $|\eta| < 5.0$. These cuts are more or less appropriate for most analyses in CMS/ATLAS. The process is dominated by the Z peak. The mechanism is rather similar to that for W production, but now the quark and antiquark are the same flavour and the x at zero rapidity is slightly higher, i.e. $x_0 = 0.0065$.

The similarity is confirmed by the results. Again all the total cross-sections using the LO generators are lower

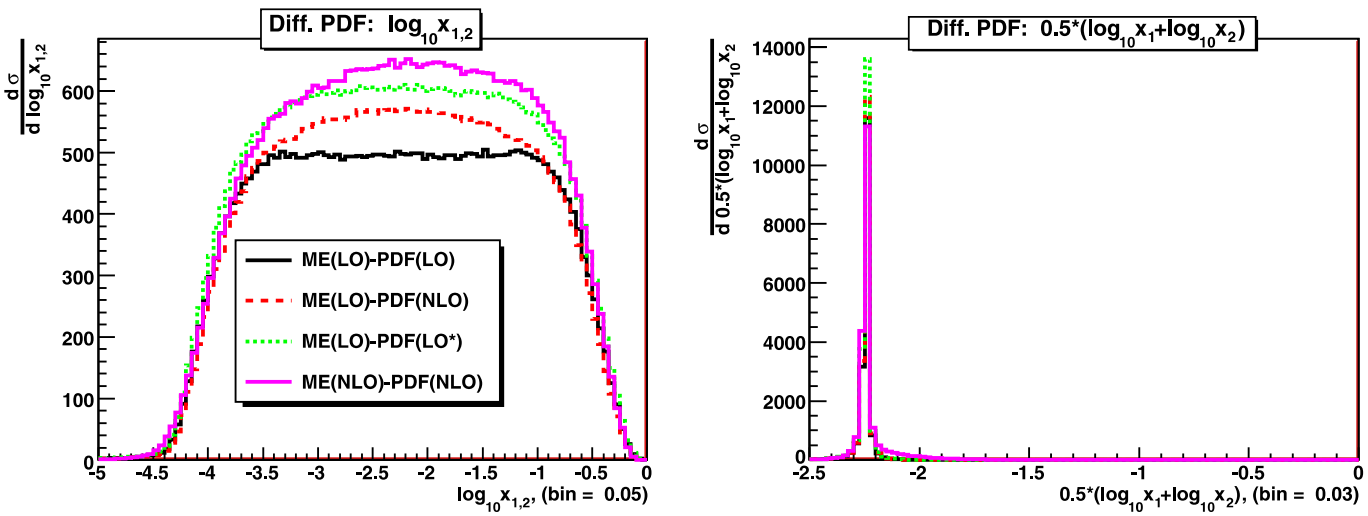

Fig. 12. The ranges in x_1 and x_2 of the contributing parton distributions for W-boson production at the LHC in the different types of calculation

than the *truth*, as seen in Table 4, but that using the LO* partons is easily closest. A similar conclusion holds for the distributions in terms of the final-state boson or the highest-$p_{\rm T}$ muon shown in the upper and lower plots of Fig. 13, respectively. For the boson the LO* partons give a quality of shapes comparable to the NLO partons, perhaps marginally better, but a better normalisation. The LO partons have the worst suppression at central rapidity, and all partons give an underestimate of the high-$p_{\rm T}$ tail. Similarly, for the muon the LO* partons give an excellent result for the rapidity distribution until $|\eta| > 4$, better in shape and normalisation than the NLO partons, whilst the LO partons struggle at central η. Again, as in W production,

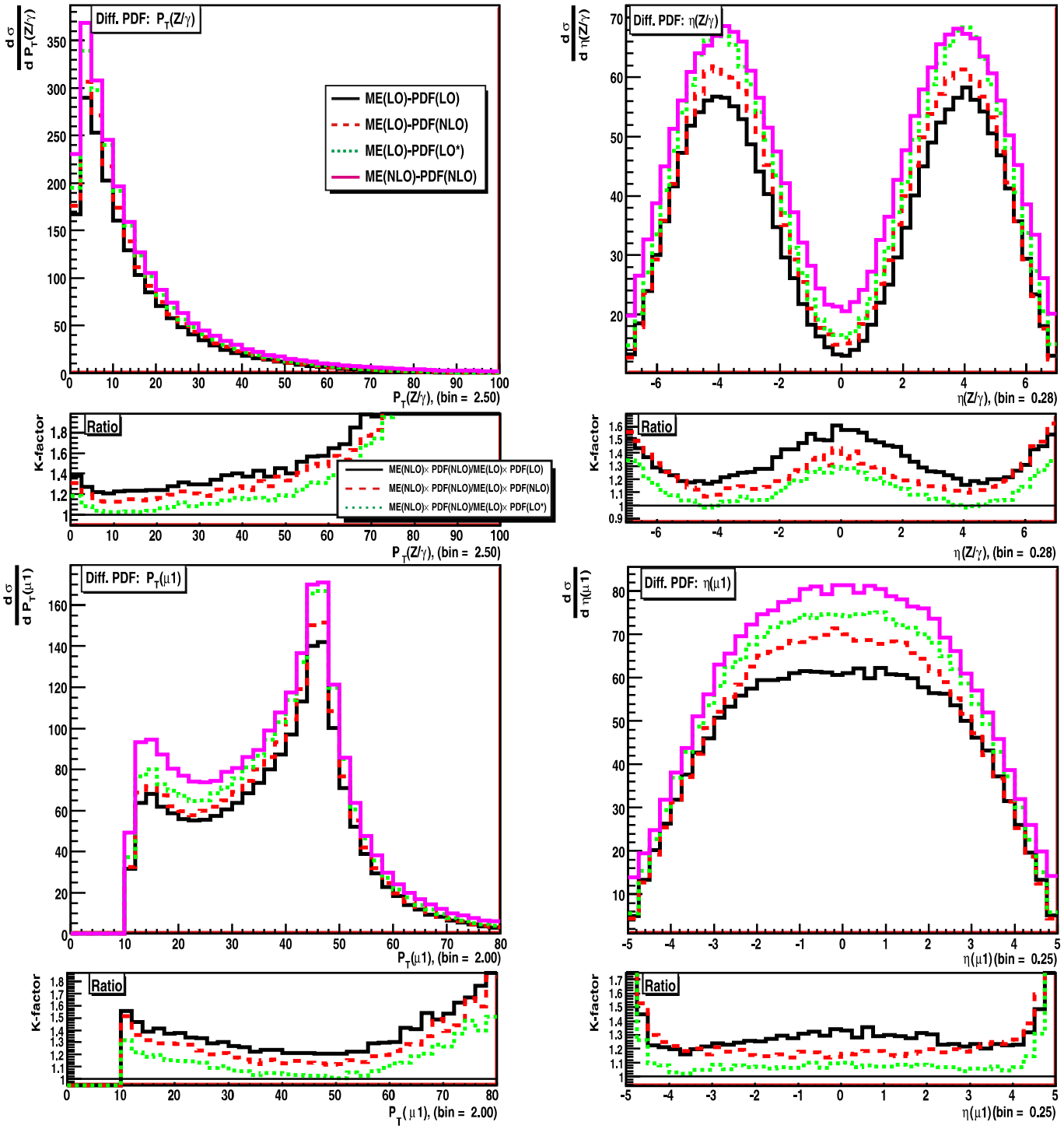

Fig. 13. The comparison between the competing predictions for the differential cross-section for Z/γ-boson production at the LHC (*upper plots*) and for the resulting highest $p_{\rm T}$ muon (*lower plots*)

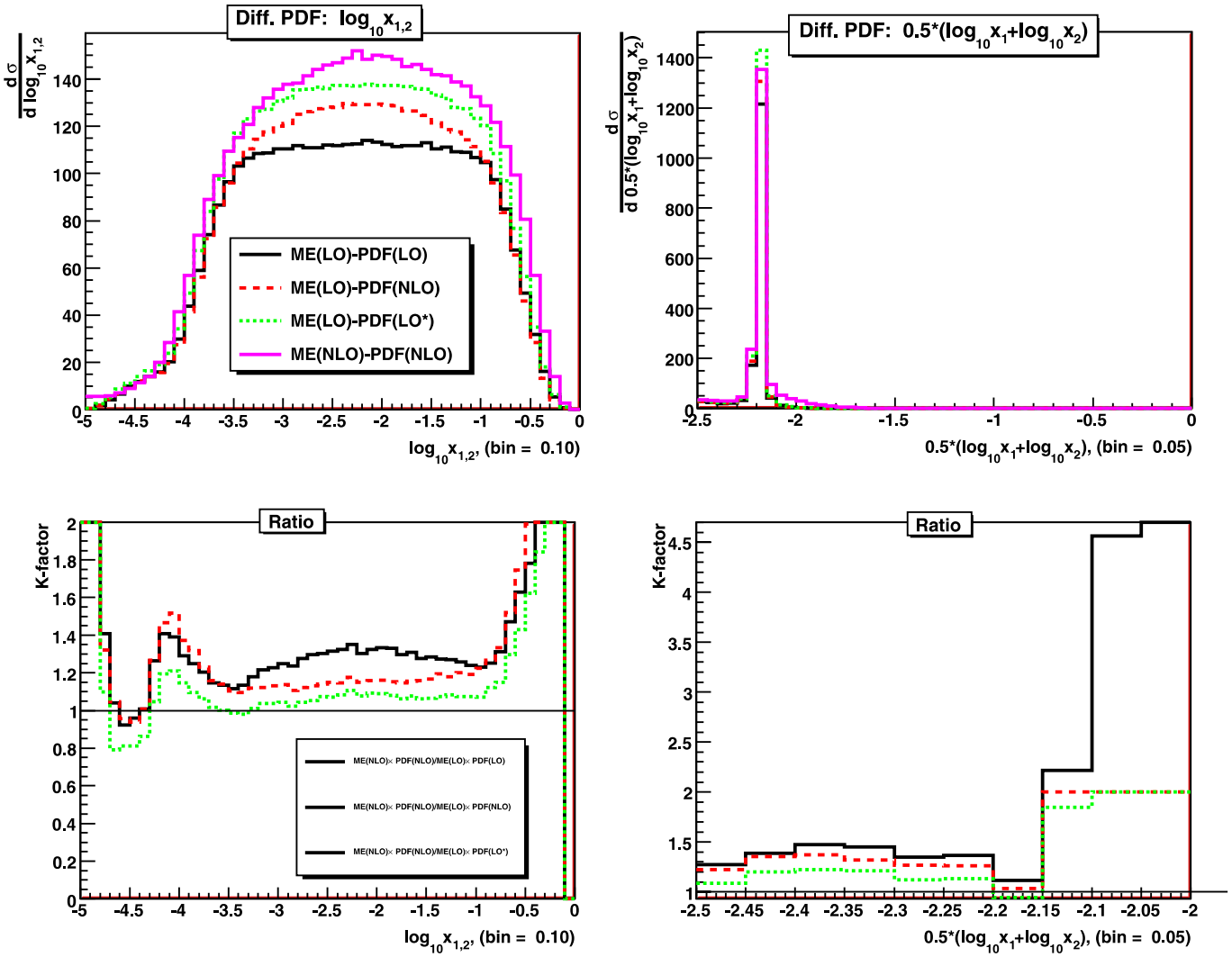

Fig. 14. The distributions of $x_{1,2}$ of the contributing parton distributions for Z/γ-boson production at the LHC in the different types of calculation

Table 4. The total cross-sections $\sigma(pp \to Z/\gamma \to \mu\mu)$ at the LHC with cuts ($p_{\rm T}(\mu) > 10$ GeV, $|\eta\mu| < 5.0$)

PDF type	Matrix element	σ (nb)	K-factor
NLO	NLO	2.40	
LO	LO	1.85	1.30
NLO	LO	1.98	1.26
LO*	LO	2.19	1.09

the $p_{\rm T}$ distribution of the muon is better than for the boson, and in normalisation is best described by the LO* PDFs.

We illustrate the ranges of x_1 and x_2 in Fig. 14. The upper right-hand plot shows that the peak in the partons contributing is indeed at $x_1x_2 = m_Z^2/s$, with some contribution from the region of higher x_1x_2. Again, this is particularly so for the case of the NLO matrix element, where one parton can make a fairly hard emission before the annihilation process. This contribution from higher x_1x_2 is most clearly seen in the lower right-hand plot. The upper left-hand plot shows the contributing x of each parton and is dominated by the line $x_1x_2 \approx m_Z^2/s$, with the plateau falling off when the quark distribution for the higher-x quark falls away for $x \to 1$, i.e. the contribution is small when $x_1 \approx 0.3$ so $x_2 \approx 0.0001$. Perhaps most interesting is the lower left-hand plot, which shows the ratio of the contribution from particular values of x for the *truth* divided by each of the LO generator calculations. In all cases the ratio diverges at very high x due to the possibility of radiation of a hard parton before annihilation at NLO. However, over the main region of contribution to the cross-section, i.e. $0.001 < x < 0.1$, the K-factor for the NLO and LO* PDFs is flat and close to 1 (though closer for the LO* PDFs), whereas there is a distinct bump to values greater than 1 for the LO PDFs. This illustrates very clearly the depletion of the quarks in this region for the LO partons and is very similar in the previous case of W production.

4.3 Single top production at the LHC

Now we consider a somewhat different process, i.e. single top production with the top decay $t \to \mu^+ + \nu_\mu + b$. At the partonic level the dominant interaction process is $qb \to qt$ (or $q\bar{b} \to q\bar{t}$), where the b-quark has been emitted from the gluon. Since the b-quark PDF is determined by evolution from the gluon PDFs, this cross-section probes both the gluon distribution and the quark distributions for invariant masses of above about 200 GeV, i.e. at central rapidity $x_0 \sim 0.01$–0.1. The t-channel nature of this process makes the invariant mass of the final state and the correspond-

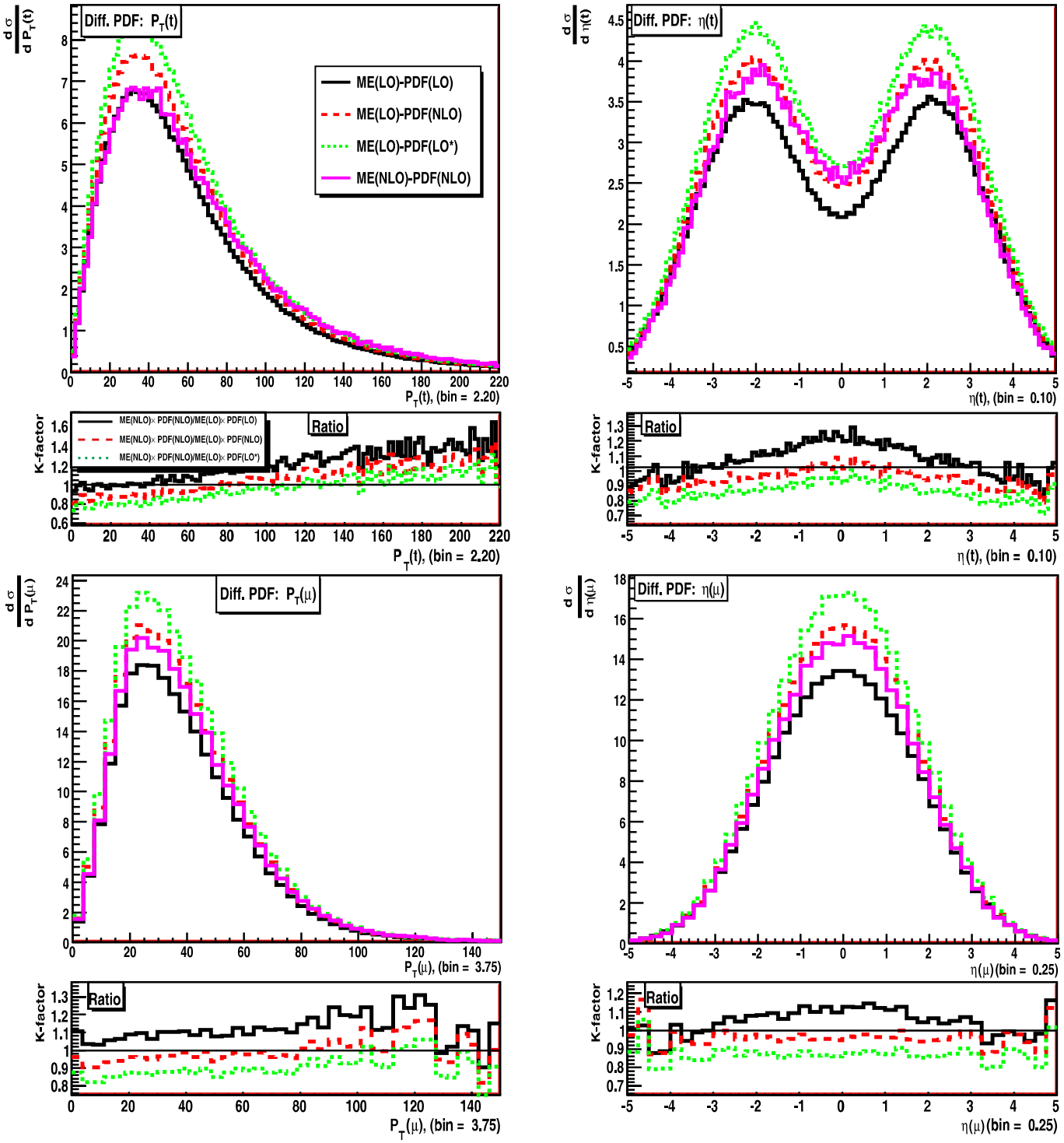

Fig. 15. The comparison between the competing predictions for the differential cross-section for single top production at the LHC (*upper plots*) and for the resulting p_{T} muon (*lower plots*)

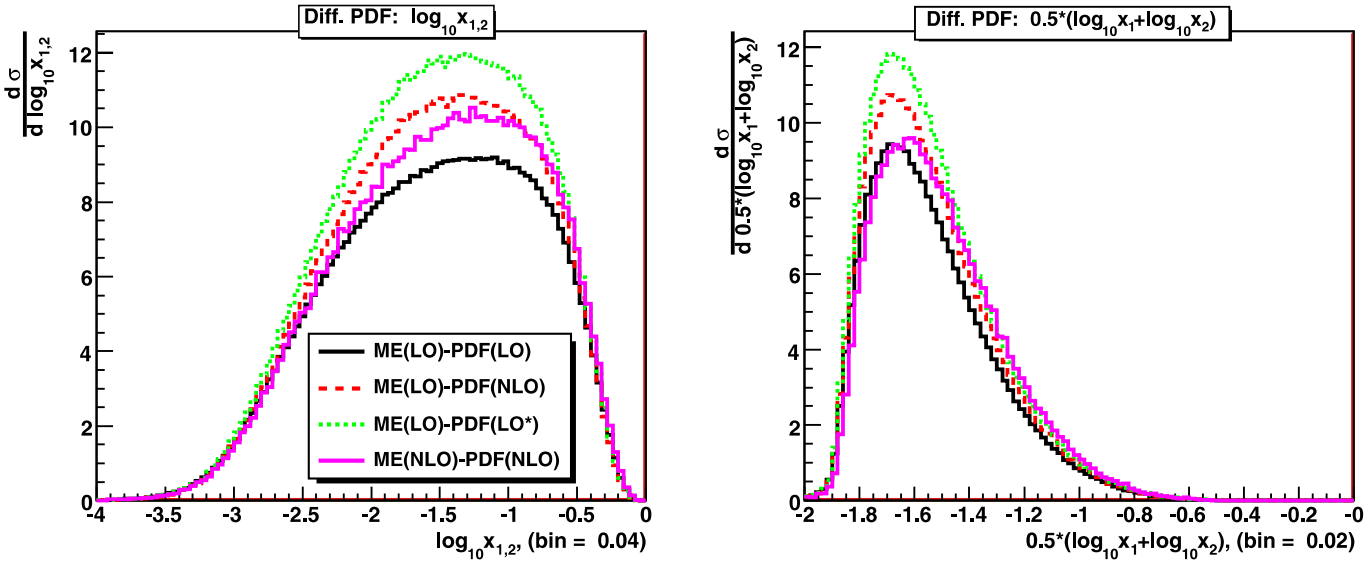

Fig. 16. The distributions of $x_{1,2}$ of the contributing parton distributions for the single top production at the LHC in the different types of calculation

ingly probed x values less precise than the previous case. The total cross-section for the various methods of calculation is seen in Table 5 (we excluded $\mathrm{Br}(t \to \mu^+ + \nu_\mu + b)$). In this case the result using the LO generators and the LO PDFs is suppressed, but that using the LO* PDFs is now larger than the *truth*. This is due to the large enhancement of the LO* gluon distribution. The NLO PDFs give the closest normalisation.

The distributions in terms of p_{T} and η of the final state top and μ originated from the top are shown in Fig. 15. For the top distribution the result using the LO generator and the LO* and NLO PDFs give a very similar result, being better than the LO PDF result both as regards normalisation and as regards shape due to the suppression of the LO quarks at central rapidities. In the case of the μ the distributions calculated with the LO generator look better than for the top, since the real NLO correction (irradiation of an extra parton) plays a lesser role for the top decay products. In this process there is a particular NLO enhancement at central rapidity, so it gives a total cross-section larger than the *truth*. In Fig. 16 we display the ranges of x sampled. The right-hand plot shows the main difference in this process as compared with the previous cases. Here we have much larger values of the "average" x.

The process also illustrates the importance of the NLO corrections in experimental analyses. If we accept the picture in which $qb \to qt$ is the LO approximation for the process,[5] the main correction comes from the gluon splitting to $b\bar{b}$, where one b-quark participates in the top production and the second b is a parton-spectator. Thus, at LO we have the b-quark in the initial state, but we assume no intrinsic b-quarks in the protons (as we pointed out the b PDFs are calculated based on the gluon distribution). It means we must produce the second b-quark somehow in any reliable simulation. Usually Monte Carlo programs generate the parton via the initial parton shower approach. It is clear that the matrix element calculation gives a more central b-quark with higher p_{T}. So, if the parton is important in an analysis, the LO approximation does not work well whatever PDF we apply.[6]

Table 5. The total cross-sections for the single top production (with top decay $t \to \mu\nu_{mu}, b$) at the LHC

PDF type	Matrix element	σ (pb)	K-factor
NLO	NLO	259.4	
LO	LO	238.1	1.09
NLO	LO	270.0	0.96
LO*	LO	297.5	0.87

4.4 Higgs production at the LHC – gluon–gluon fusion

We now consider a process that is determined entirely by the gluon distribution, i.e. the production of Higgs bosons of mass 130 GeV from gluon–gluon fusion. The cross-section depends on the gluon distribution with x at central rapidity being $x_0 = 0.01$. It is well known that there

[5] There exists another prescription, in which one considers $qg \to qt + \bar{b}$ as a LO approximation [20]. From our point of view, this approach is less motivated both from the mere vertex calculation (both Feynman graphs of the process have three vertices, whereas $qb \to qt$ has only two vertices) and availability of the b-quark PDF. The b distribution takes into account some logarithmic corrections that cannot be implemented in the LO matrix element.

[6] In fact, one can combine the LO approximation and the main real correction due to $g \to b\bar{b}$ [21, 22].

is a very large K-factor, approximately 1.7, for Higgs production via this mechanism, so it is no surprise that when using the LO generator the cross-section is suppressed by roughly this factor using both the LO and NLO PDFs, whose gluon is of a similar size for $x \sim 0.01$. However, from the right-hand side of Fig. 8 we see that the LO* gluon distribution is enhanced by a factor of ≈ 1.25 for the relevant value of x and the extra gluon contribution factor of 1.25^2 compensates for a large part of the NLO K-factor. Hence, the result using the LO* PDFs is much better than for the LO and NLO PDFs, as seen in Table 6. Since $gg \to H$ is an s-channel process, the "average" x has the same profile

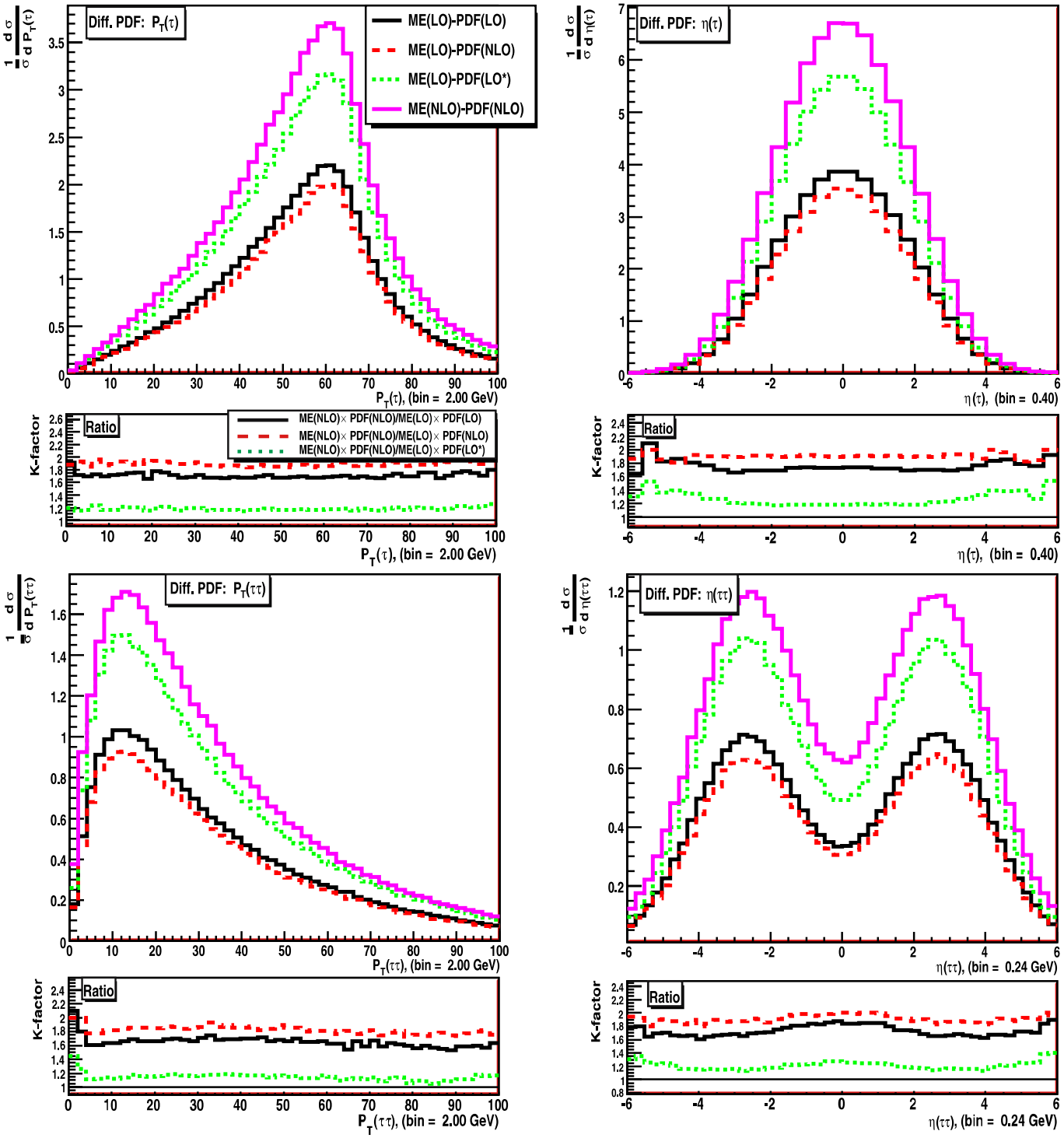

Fig. 17. The comparison between the competing predictions for the differential cross-section for the Higgs production at the LHC (*lower plots*) and for the resulting τ lepton (*upper plots*)

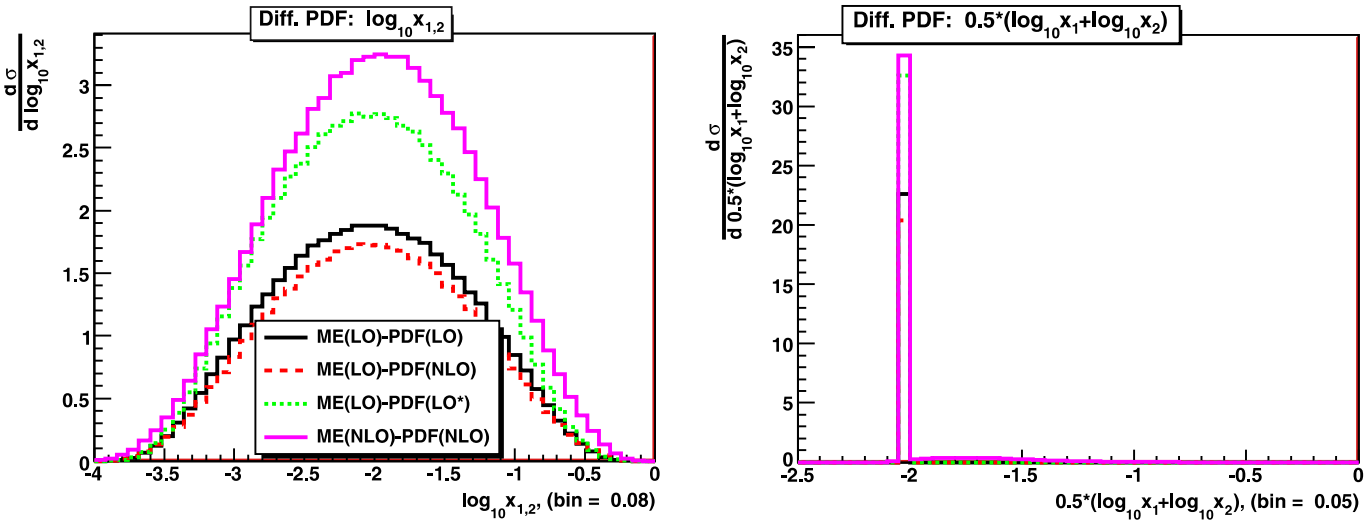

Fig. 18. The distributions of $x_{1,2}$ of the contributing parton distributions for the process $pp \to H \to \tau\bar{\tau}$ at the LHC in the different types of calculation

Table 6. The total cross-sections $\sigma(pp \to H)$ at the LHC. Strictly speaking this is $pp \to H \to \tau\bar{\tau}$ with $\mathrm{Br}(H \to \tau\bar{\tau})$ excluded

PDF type	Matrix element	σ (pb)	K-factor
NLO	NLO	38.0	
LO	LO	22.4	1.70
NLO	LO	20.3	1.87
LO*	LO	32.4	1.17

Table 7. The total cross-sections for the process $pp \to Hqq$ at the LHC

PDF type	Matrix element	σ (pb)	K-factor
NLO	NLO	4.52	
LO	LO	4.26	1.06
NLO	LO	4.65	0.97
LO*	LO	4.95	0.91

as the W and Z/γ production, as we see on the right-hand plot in Fig. 18. The distributions in the final state are shown in Fig. 17. The shapes are good in all cases, perhaps best for NLO PDFs, but the normalisation is poor except for the LO* PDFs.

4.5 Higgs production at the LHC – vector boson fusion

We again consider Higgs production, but via a different mechanism, i.e. a quark from each proton emits a vector boson that fuses to produce the final-state Higgs boson. We use quark PDFs and probe a different x region, ≈ 0.1. As we can see from Table 7, in this case the NLO K-factor is only a few percent (positive or negative), so the result using the LO generator and the NLO PDFs is only slightly above the *truth*. The result using the LO quarks is about 6% too low due to the suppression of the quarks. We note that the LO* quarks are similar to the NLO quarks for $x = 0.01$ so they give a very similar total cross-section, i.e. just a little above the *truth*. The rapidity distributions are very good using both the LO* and NLO partons as seen in Fig. 19, but we have, as usual, a small underestimate at central rapidities when using the LO PDFs. In this case the NLO corrections do little to the shape of the p_{T} distribution. The values of x probed are seen in Fig. 20 and go to quite high values of x.

4.6 Heavy quark production at the LHC

We now consider $b\bar{b}$ and $t\bar{t}$ production at the LHC. Although the dominant contribution at LO, $gg/q\bar{q} \to b\bar{b}$, does not have soft and collinear singularities (the process is called flavour creation or FCR), there are two other sources of b-quarks at hadron colliders at LO: $qb \to qb$, where the second b-quark is simulated by initial parton showers (the process is called flavour excitation, or FEX), and the QCD $2 \to 2$ process with light quarks and/or gluons, where the b-quark pair arises in the initial or final parton showers

Table 8. The total cross-sections $\sigma(pp \to b\bar{b})$ at the LHC. Applied cuts: $p_{\mathrm{T}} > 20$ GeV, $|\eta(b)| < 5.0$, and $\Delta R(b, \bar{b}) > 0.5$

PDF type	Matrix element	σ (μb)	K-factor
NLO	NLO	2.76	
LO	LO	1.85	1.49
NLO	LO	1.56	1.77
LO*	LO	2.63	1.05

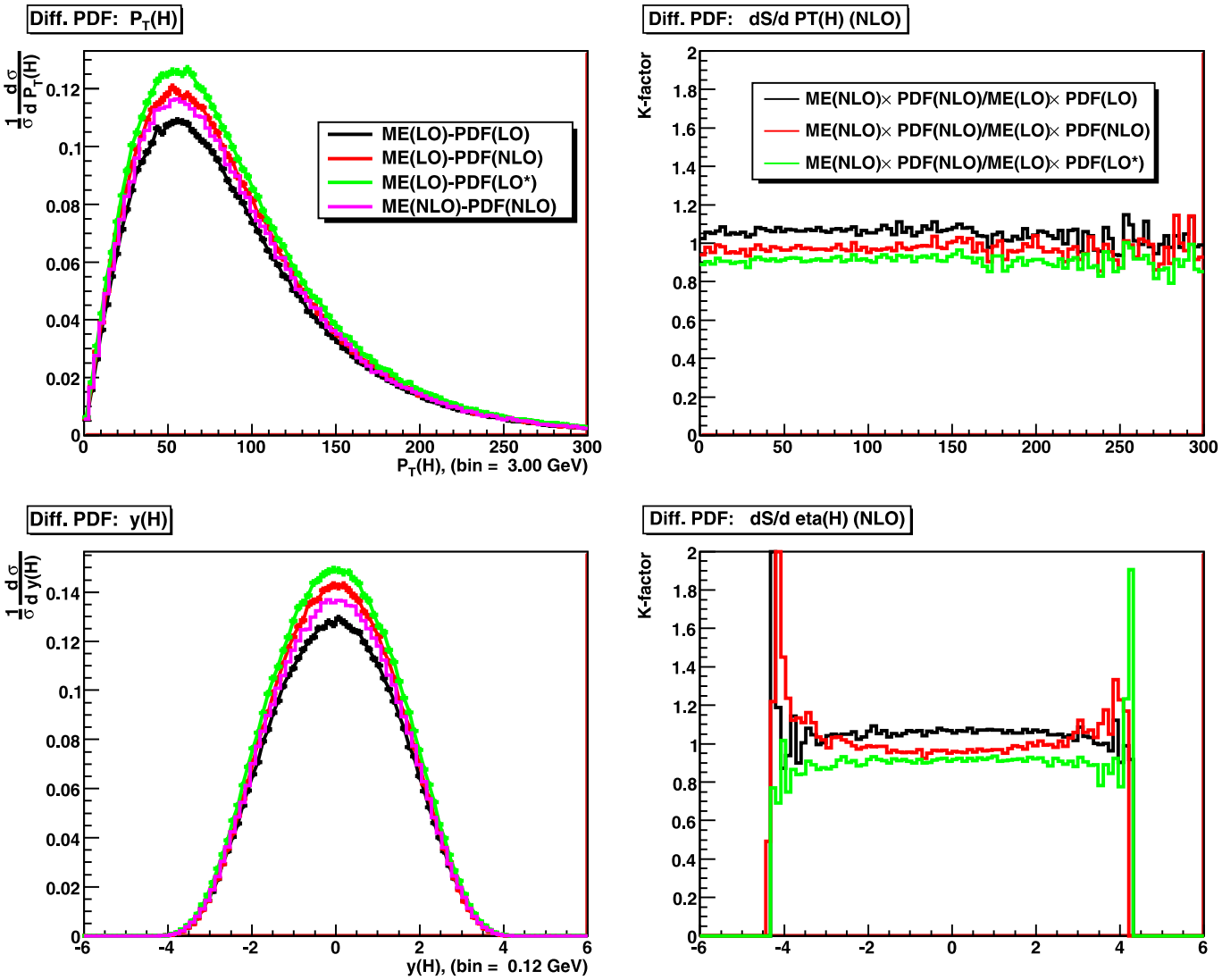

Fig. 19. The comparison between the competing predictions for the differential cross-section for the process $pp \to Hqq$ at the LHC

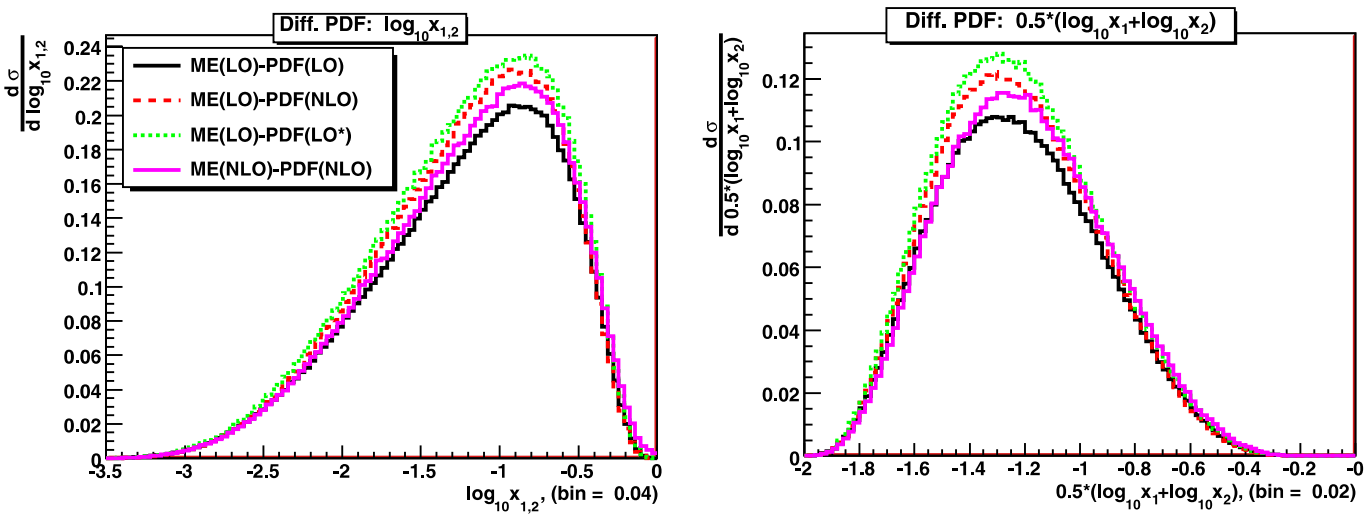

Fig. 20. The distributions of $x_{1,2}$ of the contributing parton distributions for the process $pp \to Hqq$ at the LHC in the different types of calculation

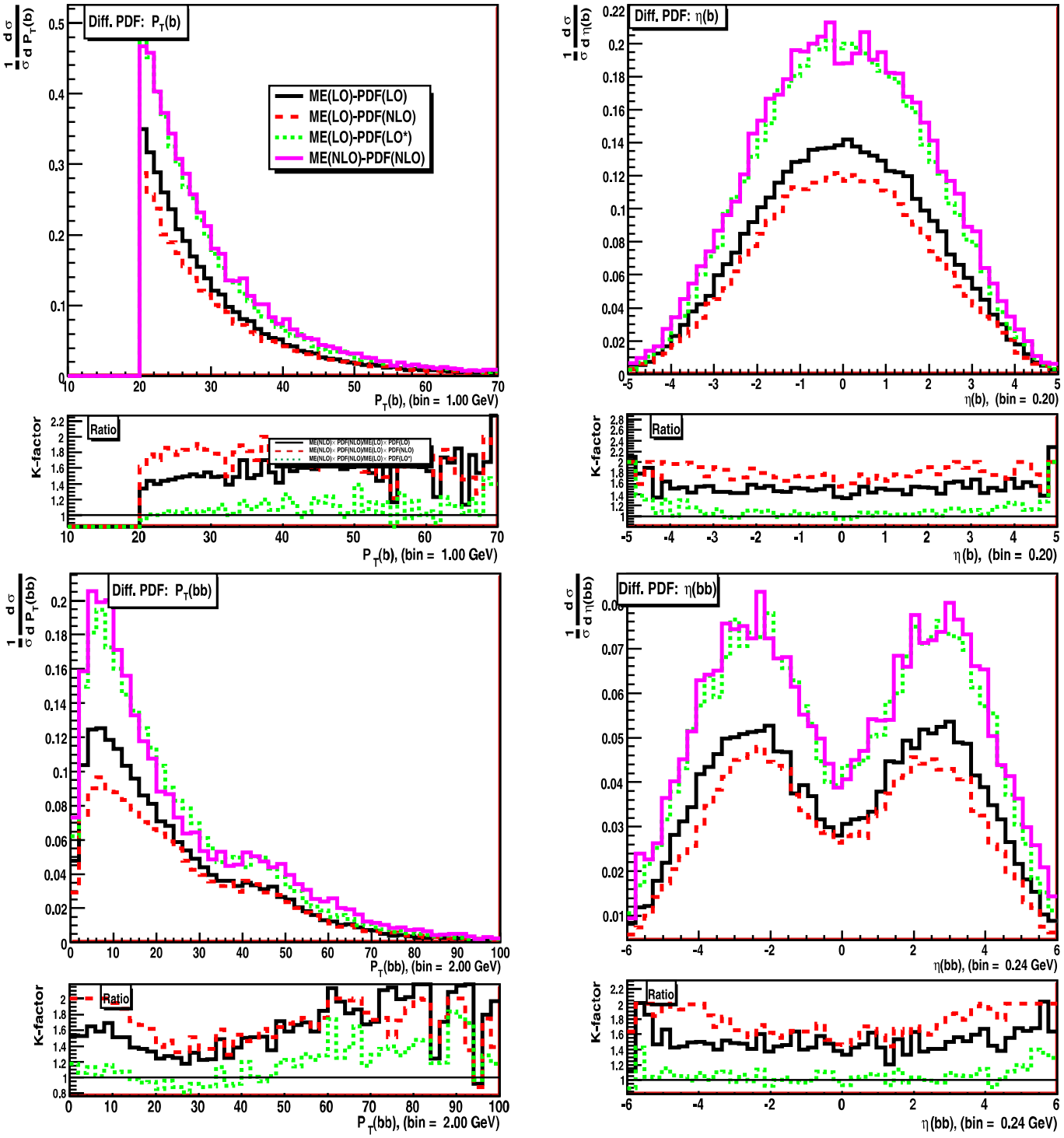

Fig. 21. Differential cross-sections for b production at the LHC (*upper plots*) and for a $b\bar{b}$ pair (*lower plots*)

(called gluon splitting or GSP).[7] These latter processes have massless partons and, thus, soft and collinear singularities. In order to exclude the dangerous regions, where the LO approximation does not work, we apply some reasonable cuts: $p_{\rm T}(b) > 20\,{\rm GeV}$, $|\eta(b)| < 5.0$ and $\Delta R(b,\bar{b}) > 0.5$. It is interesting that we cannot separate the subprocesses at NLO, so only the FCR process exists at NLO [23].

At the LHC the dominant initial state in this case is gluon–gluon, similar to the inclusive Higgs, but at much lower $p_{\rm T}$ (which dominates the total cross-section). So,

[7] For example, the total cross-section for the improved LO PDFs from Table 8 can be separated into three terms: $\sigma_{\rm tot} = \sigma_{\rm FCR} + \sigma_{\rm FEX} + \sigma_{\rm GSL}$, where $\sigma_{\rm FCR} = 1.6\,\mu$b, $\sigma_{\rm FEX} = 0.57\,\mu$b, and $\sigma_{\rm GSP} = 0.46\,\mu$b – the total cross-sections for the FCR, FEX, and GSP processes, respectively.

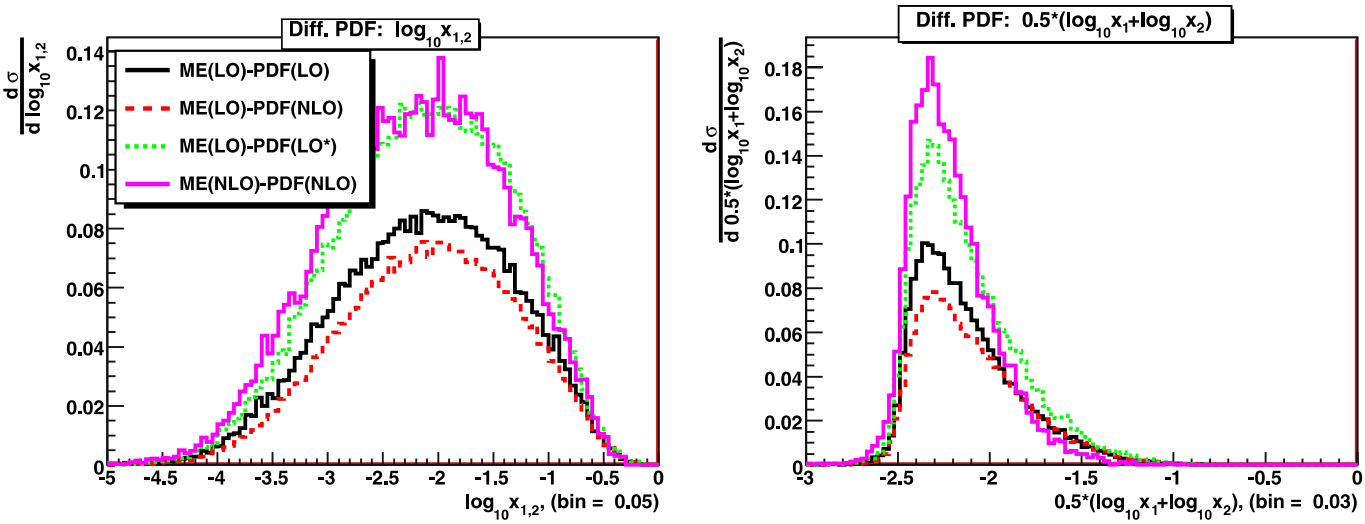

Fig. 22. The distributions of $x_{1,2}$ of the contributing parton distributions for the process $pp \to b\bar{b}$ at the LHC in the different types of calculation

in the process we probe rather low $x \sim 10^{-3}$–10^{-2} (see Fig. 22). The total cross-sections are shown in Table 8. In this case we are at low enough x to be sensitive to the small-x divergence in the NLO matrix elements, and the NLO correction is very large. All of the results obtained using the LO generator are below the *truth*, but the reduced NLO gluon means that the NLO PDFs give by far the worst result. The best absolute prediction is obtained using the LO* partons. In this case the LO gluon distribution is larger than at NLO, so LO PDFs give the second-best result.

The differential distributions in terms of p_{T} and η of a single b-quark are shown on the upper plots and for the pseudo-rapidity and p_{T} of a $b\bar{b}$ pair on the lower plots in Fig. 21. When using the LO generator the LO* PDFs do well for the single b rapidity distribution but underestimate a little at high rapidity. The LO and NLO PDFs are similar in shape, but the normalisation is worse. All PDFs obtain roughly the right shape for the $\eta(b\bar{b})$, except for a small underestimation at very high rapidity. However, for all partons there is a small problem with the shape as a function of p_{T}. Obviously, all the ratio curves become higher as p_{T} goes up. As for previous processes this happens due to the different behaviour of the additional parton generated at NLO compared to those generated by parton showers. In general, we conclude that the LO* PDFs give the best results in the comparison. Unlike the inclusive Higgs process this is not a pure s-channel process, and, as we can see in the right-hand plot in Fig. 22, there is no clear peak for the "average" x, but the main contribution in the process comes from the very low x region, near $10^{-2.5}$–10^{-2}. In this region the LO* approach works better than in the high x region.

Another interesting heavy quark production process is double top quark production. As a short check we calculated the total cross-section for the process. Table 9 reports the numbers. At the LHC this process is dominated by the gluon contribution $gg \to t\bar{t}$. For example, $\sigma_{\mathrm{ME[LO]–PDF[LO]}} = \sigma_{gg\to t\bar{t}} + \sigma_{q\bar{q}\to t\bar{t}} = 486.9\,\mathrm{pb} + 74.5\,\mathrm{pb}$. The LO* PDFs appreciably enlarge the gluonic cross-section, namely $\sigma_{\mathrm{ME[LO]–PDF[LO*]}} = \sigma_{gg\to t\bar{t}} + \sigma_{q\bar{q}\to t\bar{t}} = 622.1\,\mathrm{pb} + 77.3\,\mathrm{pb}$. Again the LO* PDFs give the best prediction.

Table 9. The total cross-sections $\sigma(pp \to t\bar{t})$ at the LHC

PDF type	Matrix element	σ (pb)	K-factor
NLO	NLO	812.8	
LO	LO	561.4	1.45
NLO	LO	531.0	1.53
LO*	LO	699.4	1.16

4.7 Jet production at the LHC

As our final example we look at high-E_{T} jet production at the LHC. In this case, as we span the range of E_{T} we span the range of x, i.e. at LO $x = E_{\mathrm{T}}/\sqrt{s}$. We also change the dominant mechanism as we change E_{T} – at the highest E_{T} quark–quark interactions are dominant while for $x < 0.1$ gluon–gluon interactions take over. In the intermediate range there is also a large contribution from quark–gluon interactions. The jet production as a function of E_{T} using the LO generator and the different PDFs as a ratio to the *truth* are shown for the lower E_{T} values in Fig. 23. For the lowest p_{T}, where we probe $x \sim 0.005$, the problems due to the relatively suppressed NLO gluon are again apparent and the LO and LO* PDFs are better in normalisation and shape than NLO. Again the LO* PDFs provide the best description, very near to the full NLO prediction as seen in Table 10. As we go to higher E_{T} the predictions largely converge, but the NLO PDFs used in the LO calculation tend to be a little small (Fig. 24).

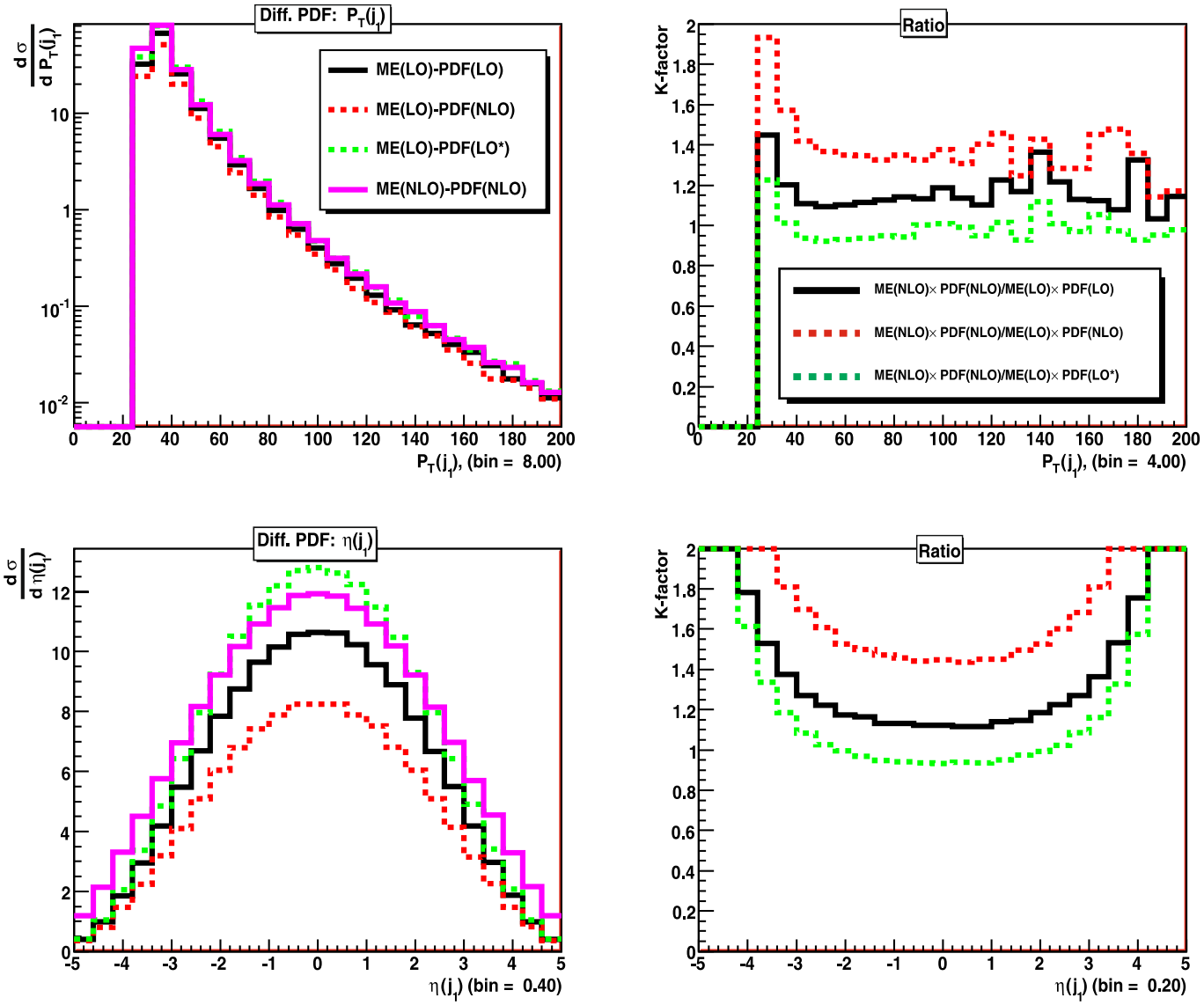

Fig. 23. Inclusive di-jet cross-section at the LHC. Differential cross-sections for the highest-Pt jet in the inclusive jet production at the LHC as a function of $p_{\rm T}$ (*upper plots*) and for η (*lower plots*)

Table 10. The total cross-sections $\sigma(pp \to jj)$ at the LHC with cuts ($p_{\rm T}(j) > 20$ GeV, $|\eta(j)| < 5.0$, $\Delta R(j,j) > 0.5$)

PDF type	Matrix element	σ (μb)	K-factor
NLO	NLO	183.2	
LO	LO	149.8	1.22
NLO	LO	115.7	1.58
LO*	LO	177.5	1.03

5 Discussion

There are a variety of reasons why the NLO cross-section corrections may be fairly large. As discussed earlier in the article, one major reason is that one probes small-x parton distributions and there appears a $1/x$ divergence in the cross-section for the first time at NLO. This is particularly the case for gluon dominated processes and is the main reason for the large corrections to the $b\bar{b}$ production at the LHC, but it also contributes to the lowest $E_{\rm T}$ jet cross-section and even probably a little to the Higgs cross-section from gluon–gluon fusion, since for the lowish mass used, gluons in the region $x < 0.001$ are probed. There are also large corrections due to soft gluon emission, which is important in regions near the edge of phase space, i.e. we have large so-called threshold corrections. These have been shown to have effects that persist some distance from the strict threshold region and also contribute to the large Higgs production correction in gluon–gluon fusion. They are the dominant reason for the large correction in $t\bar{t}$ production. There can also be a large term appearing in NLO cross-sections from the analytic continuation from the space-like region, where structure function coefficient functions are calculated to the time-like region of

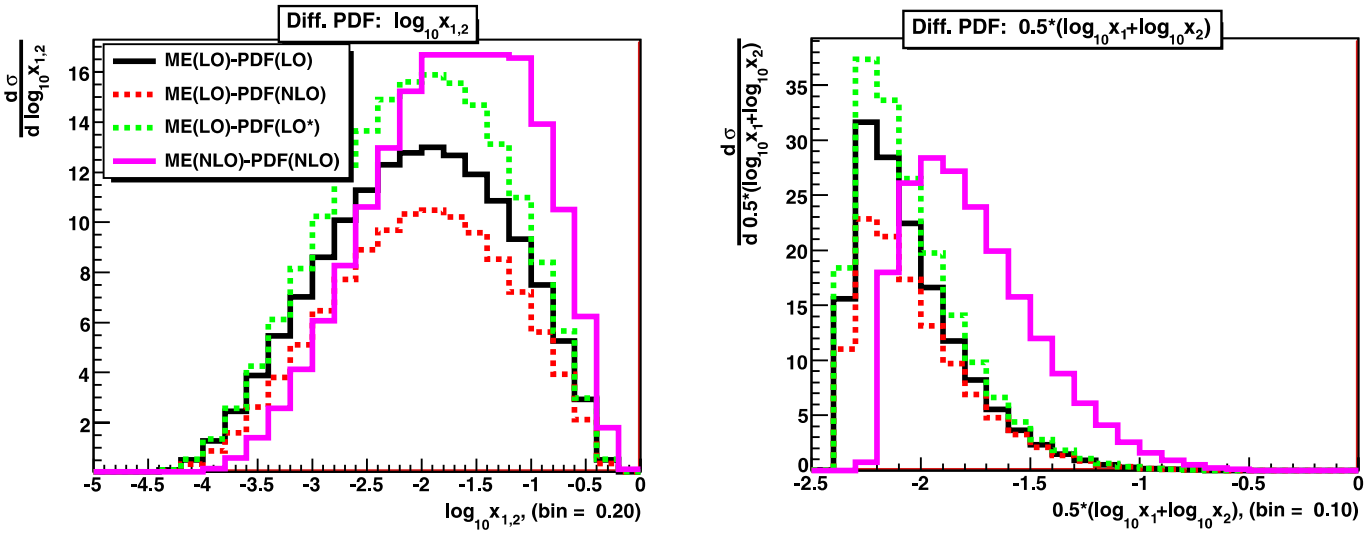

Fig. 24. The distributions of $x_{1,2}$ of the contributing parton distributions for the inclusive 2-jets production at the LHC in the different types of calculation

s-channel processes [24], and this contributes significantly to the large K-factors for W and Z production.

Hence, even if one extracted the NLO parton distributions perfectly from comparison to mainly DIS data, using them along with LO cross-sections for processes at the LHC one would expect the predictions to be generally too low, often significantly. This is indeed seen to be the case. The particular problem at small x, where the NLO gluon distribution is far too small to use with LO cross-sections, was the main motivation for introducing the LO* parton distributions, and it is no surprise that they give a far better prediction for the small-x sensitive quantities, though the high quality of the quantitative prediction is surprising. However, the relaxation of the momentum sum rule has allowed the LO* gluon distribution to be bigger than that at NLO and standard LO at most values of x, and the quarks at $x < 0.1$ driven by gluon evolution to follow suit. This actually results in the LO* parton distributions giving the best predictions for the quantities where NLO threshold corrections are large but where partons, particularly the gluon distribution, are probed for $x < 0.1$. In fact, since the parton distributions fall away very quickly above $x = 0.1$ at high scales, the region where $x \sim 0.1$ is probed is effectively near threshold. Also, the fact that the increased LO* gluon allows the quarks to be bigger than even NLO for $x < 0.01$ improves the prediction for vector boson production (particularly when an additional jet is present), compensating for the NLO correction due to analytic continuation. Overall the LO* parton distributions can qualitatively mimic the effect of the NLO cross-section corrections for a surprisingly wide variety of processes.

However, t-channel dominated processes, illustrated here by single top production and Higgs production via vector boson fusion, generally do not correspond to any of the cases where the NLO correction is expected to be large. The term from analytic continuation is not present. Moreover, a sharp threshold is not so well defined in a t-channel process, so one does not see large threshold corrections in the same way. However, the fact that there is more activity in the final state in a t-channel process than a similar s-channel process means that the "average" x probed is higher, e.g. nearly an order of magnitude for vector boson production of Higgs compared to gluon–gluon fusion, and there is less likelihood of corrections due to small-x divergences in the cross-section. Hence the absolute NLO cross-section correction is very small in these cases, the K-factor when NLO partons are used in both cases being very close to unity, and in fact slightly less. While the LO partons for the relevant $x \sim 0.1$ are smaller than at NLO, giving too small a prediction, the LO* partons are generally enhanced compared to NLO, and they give a slightly too large prediction. Hence, for our examples of t-channel processes the NLO partons are generally the absolute best to use with LO cross-sections, but one is only off by at most 10% in normalisation, with no problem with shape, using either LO or LO* parton distributions.

6 Conclusions

We have examined the effects of varying both the order of the matrix elements and the parton distributions when calculating cross-sections for particle colliders that involve hadrons. The intention is to find the best set of parton distributions to use if one only has LO matrix elements, as is often the case when using Monte Carlo generators. In order to do this we have calculated a variety of processes, both inclusive and more differential, where we can currently find the result using both NLO matrix elements and parton distributions. In the case where we look at the details of the final state, we have used Monte Carlo generators with either LO or NLO matrix elements and LO parton showering.

We notice that the NLO matrix element corrections are generally positive, and sometimes give very large enhance-

ments. In contrast, the parton distributions at NLO are sometimes bigger, but also sometimes smaller. Indeed, this must be the case since they satisfy sum rules on both parton number and momentum. The fact that higher order partonic matrix elements, and sometimes splitting functions, contain large terms in $\ln(1-x)$ and $\ln(1/x)$ means that the partons extracted in these regions at LO tend to be enhanced to make up for these missing terms. From the sum rules the parton distributions away from these regions are correspondingly generally smaller than at higher orders. In practice, there is a pronounced depletion of quarks for $x \sim 0.1$–0.001, and the large LO gluon at very small x means that it is smaller above $x \sim 0.01$. These are often the regions of most interest at hadron colliders.

A fixed prescription of either LO or NLO PDFs with LO matrix elements is unsuccessful, with each significantly out in some cases. For LO PDFs this is mainly due to the depletion just discussed, while for NLO partons the smallness in some regions compared to LO PDFs is a major problem if the large NLO matrix element is absent. This is particularly the case at very small x, where the large LO gluon compensates for the missing large NLO corrections. The best features of each order are required.

To this end we have suggested an optimal set of partons for Monte Carlos, which is essentially LO but with modifications to make the results more NLO-like, and which are called LO* PDFs. The NLO coupling is used, which is larger at low scales, and helps give a good fit to the data used when extracting partons from a global fit. The momentum sum rule is also relaxed for the input parton distributions. This allows LO PDFs to be large when it is required for them to compensate for missing higher order corrections, but not correspondingly depleted elsewhere.

We have compared the LO, NLO and LO* PDFs in LO calculations to the *truth*, i.e. full NLO, for a wide variety of processes that probe different types of PDF and ranges of x and QCD scales. In general, the results are very positive. The LO* PDFs nearly always provide the best description compared to the *truth*, especially for the s-channel processes. This is particularly the case in terms of the normalisation, but the shape is usually at least as good as – and sometimes much better than – when using NLO PDFs. It is noticeable that the type of enhancement of the PDFs provided by the allowed momentum violation seems to give a reasonably universally correct modification of the LO PDFs. Hence, while being rather crude, it seems to produce the effects obtained by modifying PDFs in a process dependent fashion for use in the Monte Carlo generators/resummations discussed in e.g. [25] (based on the calculation of the hard Wilson coefficient functions for the $Q_{\rm T}$-divergent part of the cross-sections in the context of $Q_{\rm T}$ resummation [26, 27]). In particular, it produces a relatively small enhancement of quarks and a rather larger enhancement of the gluon distribution.

It should be noted that no modification of the PDFs can hope to reproduce successfully all the features of genuine NLO corrections. In particular, we noticed the recurrent feature that the high-$p_{\rm T}$ distributions are underestimated using the LO generators, and this can only be corrected by the inclusion of the emission of a relatively hard additional parton, which occurs in the NLO matrix element correction. However, if one is limited to a strictly LO calculation, the shape as a function of $p_{\rm T}$ seems generally fairly independent of the PDF, and the normalisation is usually best with the LO* PDFs.

A preliminary version of the LO* PDFs, based on fitting the same data as in [7], is available on request from the authors. A more up-to-date version, based on a fit to all recent data, and with uncertainty bands for the PDFs, will be provided in future global fits, i.e., will follow lines similar to the MSTW07 NLO PDFs discussed in [28].

Acknowledgements. We would like to thank Jon Butterworth for asking questions which started this project; Sven Moch for encouraging further investigation for the DIS07 workshop and Claire Gwenlan for help during the early stages and for subsequent discussions and aid. We would also like to thank Paolo Bartalini, Mandy Cooper-Sarkar, Joey Huston, Alan Martin, Steve Mrenna, T. Sjöstrand, James Stirling, Graeme Watt and Bryan Webber for helpful discussions. RST would like to thank the Royal Society for the award of a University Research Fellowship. AS would like to thank the Science and Technology Facilities Council for the award of a Responsive Research Associate position, RFBR (the RFBR grant 07-07-00365-a) and the MCnet Marie Curie Research Training Network for partial support of the project.

References

1. R.S. Thorne, in: Proc. of DIS 2006, Tsukuba, April 2006 [arXiv:hep-ph/0606307]
2. R.S. Thorne, A. Sherstnev, C. Gwenlan, in: Proc. of DIS 2007, Munich, April 2007 [arXiv:0706.2131 [hep-ph]]
3. J.M. Campbell, J.W. Huston, W.J. Stirling, Rep. Prog. Phys. **70**, 89 (2007) [arXiv:hep-ph/0611148]
4. R. Field, in: TeV4LHC QCD Working Group, M.G. Albrow et al., arXiv:hep-ph/0610012
5. J. Pumplin, D.R. Stump, J. Huston, H.L. Lai, P. Nadolsky, W.K. Tung, JHEP **0207**, 012 (2002) [arXiv:hep-ph/0201195]
6. J. Kubar, M. Le Bellac, J.L. Meunier, G. Plaut, Nucl. Phys. B **175**, 251 (1980)
7. A.D. Martin, R.G. Roberts, W.J. Stirling, R.S. Thorne, Phys. Lett. B **604**, 61 (2004) [arXiv:hep-ph/0410230]
8. A.D. Martin, R.G. Roberts, W.J. Stirling, R.S. Thorne, Phys. Lett. B **531**, 216 (2002) [arXiv:hep-ph/0201127]
9. E. Laenen et al., Nucl. Phys. B **392**, 162 (1993)
10. B.W. Harris, J. Smith, Nucl. Phys. B **452**, 109 (1995)
11. T. Sjöstrand, private comments at ATLAS Generators meeting, CERN, December 2006
12. R.S. Thorne, Phys. Rev. D **73**, 054019 (2006)
13. S. Frixione, B.R. Webber, JHEP **0206**, 029 (2002) [arXiv:hep-ph/0204244]
14. CompHEP Collaboration, E. Boos et al., Nucl. Instrum. Methods A **534**, 250 (2004) [arXiv:hep-ph/0403113]
15. A.S. Belyaev et al., arXiv:hep-ph/0101232
16. G. Corcella et al., JHEP **0101**, 010 (2001) [arXiv:hep-ph/0011363]
17. W.T. Giele, E.W.N. Glover, D.A. Kosower, Nucl. Phys. B **403**, 633 (1993) [arXiv:hep-ph/9302225]

18. T. Figy, C. Oleari, D. Zeppenfeld, Phys. Rev. D **68**, 073 005 (2003) [arXiv:hep-ph/0306109]
19. J. Campbell, R.K. Ellis, Phys. Rev. D **65**, 113 007 (2002) [arXiv:hep-ph/0202176]
20. T. Stelzer, Z. Sullivan, S. Willenbrock, Phys. Rev. D **56**, 5919 (1997) [arXiv:hep-ph/9705398]
21. E.E. Boos, V.E. Bunichev, L.V. Dudko, V.I. Savrin, A.V. Sherstnev, Phys. Atom. Nucl. **69**, 1317 (2006)
22. E.E. Boos, V.E. Bunichev, L.V. Dudko, V.I. Savrin, A.V. Sherstnev, Yad. Fiz. **69**, 1352 (2006)
23. S. Frixione, P. Nason, B.R. Webber, JHEP **0308**, 007 (2003) [arXiv:hep-ph/0305252]
24. G. Parisi, Phys. Lett. B **90**, 295 (1980)
25. S. Mrenna, arXiv:hep-ph/9902471
26. C.T.H. Davies, W.J. Stirling, Nucl. Phys. B **244**, 337 (1984)
27. J.C. Collins, D.E. Soper, G. Sterman, Nucl. Phys. B **250**, 199 (1985)
28. R.S. Thorne, A.D. Martin, W.J. Stirling, G. Watt, in: Proc. of DIS 2007, Munich, April 2007 [arXiv:0706.0456 [hep-ph]]